# DEEP EUTECTIC SOLVENT SUPPORTED POLYMER-BASED HIGH PERFORMANCE ANION EXCHANGE MEMBRANE FOR ALKALINE FUEL CELLS

**Aida Barlybayeva**, BSc

**Submitted in fulfillment of the requirements**
**for the degree of Master of Science**
**in Chemical and Materials Engineering**


**School of Engineering and Digital Sciences**
**Department of Chemical and Materials Engineering**
**Nazarbayev University**

53 Kabanbay Batyr Avenue,
Astana, Kazakhstan, 010000

**Supervisors:** Almagul Mentbayeva, PhD, Assistant Professor
Bauyrzhan Myrzakhmetov, PhD, Senior Researcher

**April 26th, 2024**

DECLARATION

I hereby, declare that this manuscript, entitled *"Deep Eutectic Solvent Supported Polymer-Based High Performance Anion Exchange Membrane for Alkaline Fuel Cells"*, is the result of my own work except for quotations and citations which have been duly acknowledged.

I also declare that, to the best of my knowledge and belief, it has not been previously or concurrently submitted, in whole or in part, for any other degree or diploma at Nazarbayev University or any other national or international institution.

---

Name: Aida Barlybayeva

Date: April 26th, 2024

# Abstract

Deep eutectic solvent (DES)-supported polymer-based anion-exchange membrane (AEM) was prepared by a new approach, where a crosslinked poly(vinyl) alcohol (PVA)-based nanofiber mat was impregnated with DES by soaking method. A PVA-based nanofibers were obtained using electrospinning method and crosslinked with glutaraldehyde (GA) in concentrations ranging from 4 wt.% to 8 wt.%. DES was synthesized by mixing choline chloride (ChCl) and ethylene glycol (EG) at a molar ratio of 1:3, respectively. Electrochemical characterization of AEM modified with DES (DES3@PVA4) revealed a conductivity of 0.66 and 1.05 mS/cm at room temperature and 60 $^{o}$C, respectively. Moreover, the absence of swelling and a significant improvement in elongation at break were identified from 0.24 to 1.08 %. Thus, the DES-supported PVA-based composite membrane demonstrated high hydroxide conductivity, flexibility, and mechanical stability in a fully hydrated state, showing potential to be utilized as an AEM for alkaline fuel cell (AFC) applications.

# Acknowledgments

This work was carried out under a research project titled AP14869880, “Deep Eutectic Solvent Supported Polymer-Based High-Performance Anion Exchange Membrane for Alkaline Fuel Cells,” funded by the Ministry of Education and Science of Kazakhstan. The Principal Investigator of the project and lead supervisor is an Assistant Professor of the Chemical and Material Engineering (ChME) Department, Almagul Mentbayeva, and the Co-Principal Investigator is an Associate Professor, Yanwei Wang. The co-supervisor is a Senior Researcher, Dr. Bauyrzhan Myrzakhmetov.

Firstly, I would like to express my immense gratitude to Assistant Professor Almagul Mentbayeva, Associate Professor Yanwei Wang, and Dr. Bauyrzhan Myrzakhmetov for leading my research pathway and giving me valuable experience in writing the literature review and conducting experiments. All the people mentioned above contributed their ideas to improve my work, which was only possible with their careful supervision. My co-supervisor has given me great help and support and shared advice on fabrication methods and membrane characterization tests.

Last but not least, I am very grateful to Nazarbayev University for providing me with brilliant knowledge, new friends, student life memories, and the opportunity to get a master's degree.

# Table of Contents

# List of Abbreviations

| | |
|---|---|
| AEM | Anion-exchange membrane |
| AEMFC | Anion-exchange membrane fuel cell |
| AFC | Alkaline fuel cell |
| CA | Citric acid |
| ChCl | Choline chloride |
| CS | Chitosan |
| DES | Deep eutectic solvent |
| DI | Deionized (water) |
| EG | Ethylene glycol |
| EIS | Electrochemical impedance spectroscopy(e) |
| ETFE | Poly(ethylene-co-tetrafluoroethylene) |
| FC | Fuel cell |
| FTIR | Fourier transform infrared spectroscopy(e) |
| GA | Glutaraldehyde |
| HBA | Hydrogen bond acceptor |
| HBD | Hydrogen bond donor |
| HDTB | Hexadecyltrimethylammonium bromide |
| IL | Ionic liquid |
| MCFC | Molten carbonate fuel cell |
| NADES | Natural deep eutectic solvent |
| PAFC | Phosphoric acid fuel cell |
| PDDA | Poly(diallyldimethylammonium chloride) |
| PEM | Proton-exchange membrane |
| PEMFC | Proton-exchange membrane fuel cell |
| PTFE | Polytetrafluoroethylene |

| | |
|---|---|
| PVA | Poly(vinyl) alcohol |
| QA | Quaternized ammonium |
| QPVA | Quaternized poly(vinyl) alcohol |
| SEM | Scanning electron microscopy(e) |
| SOFC | Solid oxide fuel cell |
| SR | Swelling ratio |
| SS | Stainless steel |
| TEM | Transmission electron microscopy(e) |
| TG | Thermogravimetric |
| TGA | Thermogravimetric analysis |
| EUTM | Electronic universal testing machine |
| WU | Water uptake |

# List of Tables

# List of Figures

# Chapter 1 - Introduction

## 1.1 General

A new fabrication approach for DES-supported AEMs for AFC application was developed, and the effect of DES impregnation on ionic conductivity and mechanical stability was analyzed. The obtained composite AEMs comprise a PVA polymer-based nanofibrous network prepared by the electrospinning method and impregnated with DES, which consists of ChCl and EG. Composite membranes obtained by this fabrication procedure guaranteed high performance by enhanced ionic conductivity and mechanical stability according to AEM requirements.

## 1.2 Aim and Objectives

DES might facilitate the conductivity of hydroxide ions, while the polymer-based nanofibers in the form of membranes are the platform for ion conduction. This project aims to fabricate highly conductive and mechanically stable DES-supported PVA-based composite AEMs for AFC application using the electrospinning technique. The objectives to fulfill this aim are as follows:

1. To crosslink PVA nanofibers fabricated by electrospinning technique using a cross-linking agent.
2. To modify crosslinked PVA-based membranes by impregnation with DES.

## 1.3 Methodologies and Techniques

The central concept of the fabrication procedure is based on the electrospinning method, which allows the fabrication of a network of fibers on a micro/nanometer size scale. The working principle is based on producing an electrical field between a drop of polymer solution on a nozzle and a grounded collector when a high voltage is applied, generating a Taylor cone. Once the repulsive forces exceed the polymer droplet’s surface tension, a critical point is achieved by activating the electric field, resulting in the spraying of a solution jet from the Taylor cone’s head. It evaporates or solidifies, creating a network of nanofibers before reaching the collector [1]. Processing parameters, such as polymer flow rate, applied voltage, and the nozzle tip-to-collector distance, significantly determine the formation of electrospun fibers and control their diameters.

Along with the external parameters, the parameters of the polymer solution, such as molecular weight, concentration, and viscosity, can impact the quality of nanofibers obtained via electrospinning [2]. Enhancing mechanical characteristics by uniaxially aligning polymer chains inside nanofibers is one of the advantages of the electrospinning process. In addition, electrospinning can enhance the conduction of ions by creating interrelated channels, which corresponds to the aim of this research [1,3]. Therefore, the materials prepared using the electrospinning technique could be used as a part of AEM for AFC application.

# Chapter 2 – Literature Review

## 2.1 Fuel cells

Fossil fuels produce considerable greenhouse gases, which have increased global warming. Furthermore, the quick depletion of natural gas and oil supplies poses a severe problem for the future. FCs are the alternative energy option promised the most among the several potential possibilities because they have a limitless capacity to produce electricity as long as the fuel injection remains active. They convert chemical energy into electrical energy via an electrochemical reaction between the fuel and oxidant, where the byproducts are heat and water. FCs are operating with higher efficiency and lower emissions than conventional combustion-based technologies [4,5]. PAFCs, MCFC, SOFCs, AFCs, and PEMFCs are the main models of FCs available today. Operating temperature, particular field of operation, design, and the type of electrolyte employed are the essential variations between the numerous fuel cell types. Researchers have made many attempts to computationally investigate SOFCs, PAFCs, and MOFCs using various software [6-8]. Still, experimentally, there is an opportunity to study them for PEMFCs and AFCs. Table 2.1 summarizes their main characteristics [9].

Table 2.1 The primary characteristics distinguishing various FC types [9]

| **FC** | **Operating temperature, $^{o}$C** | **Electrolyte** | **Catalyst** | **Electrical efficiency** |
|---|---|---|---|---|
| AFC | <90 | KOH solution | Transitions metals | 60-70 % |
| PEMFC | <80 | PEM | Pt/Pt alloy | 40-60 % |
| SOFC | 800-1000 | Oxide ion conducting ceramic | Cermet (combined with Ni) | 60-65 % |
| MCFC | 620-660 | Molten mixture of alkali metal carbonates | Non-precious metals | 65 % |
| PAFC | 160-220 | Phosphoric acid | Pt | 55 % |

According to Table 2.1, PEMFCs and AFCs can be emphasized because of their lowest working temperature, approximately 80-90 $^{o}$C, along with elevated electrical efficiency of approximately 60 % compared with other types [9].

### 2.1.1 PEMFCs and AEMFCs: advantages and disadvantages

PEMFCs are the most developed and widely used type of FCs due to their sufficient power density, rapid startup, long durability, and accessibility of proton-conducting commercial membrane Nafion with excellent mechanical/chemical stability and high proton conductivity [10-12]. For instance, at 80 °C and 100 % relative humidity, Nafion has a sufficient conductivity of protons of around 0.1 S/cm. This membrane may be fabricated very thin (20-25 μm) with enhanced mechanical stability [13]. PEMFCs' high proton conductivity is characterized by the size of the $H^+$ ion ($10^{-15}$ m), which is significantly smaller than the size of the $OH^-$ ion ($10^{-10}$ m). Therefore, protons are transported much quicker through PEM than hydroxide ions through AEM [5].

However, some aspects of PEMFC's performance limit its range of applications. Key challenges are limitted fuel selection, the high price of platinum group catalysts to promote electrochemical processes, and fuel crossover associated with a transfer of undesired gas across the membrane [14,15].

As a result of these drawbacks, the focus should be turned to FCs known as AFCs that could operate in an alkaline environment. Moreover, it is considered a viable option along with PEMFCs because of the similar range of operating temperatures required [9,10]. Thus, compared with platinum-based catalysts intended for PEMFCs, more affordable transition-metal catalysts may improve the functioning of AFCs due to their different ion transport processes [16]. Other benefits include using a wide range of fuels, the excellent resistance to corrosion of widely applied cell material components in the alkaline medium, improved cell voltage, low fuel crossover caused by the hydroxide ion and fuel moving in the opposite directions, and faster oxygen reduction kinetics [17].

The electrolyte used most frequently in AFCs is potassium hydroxide (KOH) solution, which is the most conductive and cheap electrolyte. Nevertheless, there are potential threats of leakage or electrolyte drying. In addition, this electrolyte effortlessly combines with $CO_2$ due to its high sensitivity and, as a result, creates carbonates such as $K_2CO_3$. Although the presence of KOH accelerates the rate of hydroxide ions' conductivity, at the same time, it reduces their amount

and simultaneously lowers ionic conductivity and power output [18]. Using AEMs instead of a liquid electrolyte as a solid polymer electrolyte has more advantages. It was developed as a part of AEMFCs. Its polymer-based nature makes it possible to prevent $CO_2$ poisoning and leaks.

The scheme of working principle of both PEMFC and AEMFC is shown in Figure 2.1 [10].

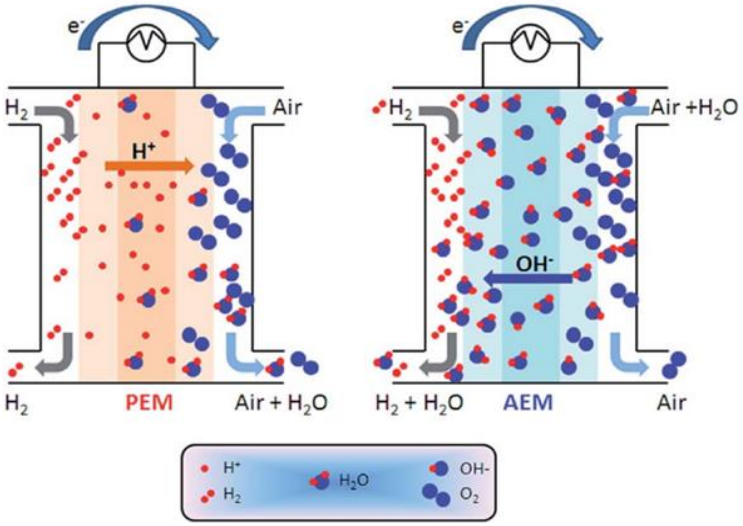


Figure 2.1 Working principle of PEMFC and AEMFC [10].

Both PEMFC and AEMFC consist of an electrolyte membrane, cathode, and anode. The anode's purpose is to provide and oxidize hydrogen, and the cathode's purpose is to reduce oxygen. In PEMFC, protons are carried across the PEM from the anode to the cathode, wherein electrons are transported through an external circuit load, unlike AEMFC, which transports hydroxide ions from the cathode to the anode. The overall reaction and potential are identical in both cases, but the half-reactions differ. For example, in a PEMFC, oxygen combines with protons and electrons on the cathode to produce heat and water as a byproduct. For AEMFC, oxygen is reduced on the cathode to develop $OH^-$ ions. These ions oxidize when combined with hydrogen fuel at the catalyst side of the anode to produce water accompanied by electrons [10].

Regarding analysis provided, there is the main point why AFC should be considered, specifically AEMFC as the main object of study. Due to using less expensive catalysts, AEMFC could be a viable alternative to PEMFC. However, it still has lower ionic conductivity and stability than PEMFC and is not yet to be widely commercialized. The main challenge for AEMFCs is that they do not have standard commercially accessible materials or defined baseline procedures (test

conditions and properties), unlike PEMFCs, which have undergone extensive research [19]. So, there is a need to conduct research based on AEM's modification for the prospective commercialization of AEMFC.

## 2.2 Anion exchange membrane

According to Ran et al. [20], an essential part of alkaline fuel cells, AEMs are crucial as gas barriers, electron insulators, and ion conductors. They comprise a polymer backbone, moveable counter-ions, additives, and immobilized charge groups functionalized with cation to conduct hydroxide ions [20].

AEMs must satisfy the following requirements for the successful commercialization and widespread application of AEMFCs [18, 21]:

1. sufficient $OH^-$ conductivity (>100 mS/cm);
2. the membrane thickness should be in the 50-80 μm range;
3. sufficient current density (> 0.5 $A/cm^2$);
4. stability in alkaline solution at high temperatures;
5. complete insulation of electrons;
6. exceptional mechanical, thermal, and chemical stability during manufacturing and operation;
7. low cost and availability.

Much research is being conducted to fulfill these requirements, mainly based on increasing ionic conductivity and chemical and mechanical stability. Despite this, it is challenging to achieve all these requirements to a great extent at the same time. For example, increasing the amount of membrane charge groups can lead to higher ionic conductivity. However, this usually weakens mechanical stability due to excessive WU and SR [21].

### 2.2.1 Preparation of AEM

To date, numerous AEM synthesis procedures have been pursued to produce AEMs with increased efficiency for AEMFCs. The fabrication and improvement of AEMs involves:

1. choosing new materials for the polymer backbone [22];

2. functionalizing of polymer backbone using different either cations or functional groups for conduction of hydroxide ions [23];
3. processing polymer-based solutions by using various approaches and membrane fabrication procedures [24-26];
4. using various additives to improve membrane performances [27].

#### 2.2.1.1 Fabrication methods

Among various research papers, only two membrane casting methods are the most common and were successfully implemented: solution casting and electrospinning. Numerous attempts have been made to use the solution casting technique to create polymer-based electrolyte membranes characterized by excellent ionic conductivity and vital membrane/electrode interactive properties. These techniques produced membranes with poor ion conduction channels, lower porosity, and low-order pore sizes [25,26]. Therefore, researchers are now actively using electrospinning to create polymer-based nanofibers by regulating fiber shape, diameter, and porosity that could serve as host matrices for polymer electrolytes [28]. Electrospinning may fabricate AEMs that are more mechanically stable, have higher porosities, and have a narrower particle size distribution, all of which help the electrode and electrolyte make contact, increase hydroxide ion conduction, and enhance the efficiency of the FC device.

### 2.2.2 Materials for AEM

#### 2.2.2.1 Polymer backbones for AEM

As was mentioned, AEMFC operation depends significantly on the choice of material for AEM. In addition, AEM fabrication could be expensive, complex, and less environmentally friendly since specific polymers dissolve in costly and detrimental environment organic solvents under elevated temperature ranges and could require intricate preparation [19].

Aliphatic polymer backbones are preferred the most, and they involve the most widely used polymers, such as PVA [29], PTFE [30], ETFE [31], and CS [32]. For instance, it has previously been suggested that naturally occurring materials like CS are promising. Since it is strongly preferred that the material be non-toxic, environmentally benign, and bio-renewable [16]. Even with all of the advantages discussed, CS-based AEMs are still not as beneficial as synthetic AEMs,

particularly regarding mechanical properties (which can be enhanced by adding fillers) and ionic conductivity (which has only reached $10^{-2}$ S/cm) [33].

In considering the advantages that PVA possesses over the other polymers, PVA has been the most widely used synthetic polymer for AEM. These benefits include biodegradability, water solubility, non-toxicity, high ability to form fibers, and high thermal and chemical stability. However, the limitation in the wet state results in low mechanical strength, which can be overcome by adding additives [29].

#### 2.2.2.2 Functional charge groups for AEM

Quaternary ammonium (QA) groups [34] are the most extensively investigated ion-functionalized charge groups because of their easy functionalization, reasonable alkaline stability and cost, and comparatively high ion conductivity. However, because of the degradation caused by Hofmann elimination, ylide formation, and nucleophilic substitution, the QA groups are not stable in alkaline solutions, specifically at elevated temperatures [35]. QA groups remain prevalent in AEMs, where early chemical stability problems have been resolved using cross-linking methods. Also, AEMs have been developed using several functionally charged groups, such as imidazolium [36], phosphonium [38], guanidium [37], pyridinium [39], and sulfonium [40], in order to get beyond the QA limits in AEMFC use.

### 2.2.3 Modifications of PVA-based AEM research progress

A wide variety of PVA-based AEMs have been produced to date. Numerous perspectives have investigated the increase in the efficiency of AEMs for FC improvement. PVA, the backbone polymer, was frequently mixed with alternative polymers, treated with a variety of additives, such as crosslinkers/fillers, and fabricated using multiple methods and processes.

Gopi and Bhat in 2017 [41] published successful research where functionalized with QA groups, PVA was used as a material for AEM for AFC applications. This work investigated PVA quaternization with HDTB added in different weight percentages (wt.%). They used the solution casting method for membrane preparation, but before that, they conducted in situ cross-linking with GA chemically and thermally. This means they used an additive to control the WU and SR and increase the membrane's stability in an alkaline medium. As a result, they provided the figure, where their ionic conductivity results were compared with other literature, and ionic conductivity

was 4.84 mS/cm at 30 $^{o}$C. Even after 300 hours in 4M KOH at 80 $^{o}$C, the improved QPVA membrane maintains 80 % of its conductivity and ion exchange capacity with an SR of 25 %, according to the alkaline stability of the membrane [41].

In comparison with Gopi and Bhat, Samsudin et al. in 2022 [42] prepared polymer composite membranes composed of nanofiber mats of QPVA and a combination of PDDA and QPVA prepared at different mass ratios as a filler, which means they implemented an electrospinning method. Interfiber voids of the QPVA nanofiber mat were modified using the filler mentioned above since fuel crossover requires a densely integrated fiber membrane. The commercial QPVA was applied to prepare the fibers. This work also did cross-linking by immersion of QPVA fiber mats in GA solution and repeated with QPVA-PDDA dense membrane. As a result, Samsudin et al. have achieved the most significant WU, ion exchange capacity, and $OH^-$ conductivity of QPVA/PDDA (1:0.5) AEM prepared by electrospinning with values 57.6 %, 0.93 mmol/g, and 43.67 mS/cm at 80 $^{o}$C, respectively [42]. These values are higher than PVA/PDDA AEMs prepared by the solution casting method from another literature (1.02 mmol/g and 35.5 mS/cm at 60 $^{o}$C) [43]. Moreover, the obtained AEM showed strong alkaline stability with a 5% loss in conductivity after undergoing extreme conditions (6M KOH and 80 $^{o}$C) for 360 hours [42].

According to the articles mentioned above, they had the same problem with the membrane's ionic conductivity and chemical stability in an alkaline medium, and the appropriate approach was found. Also, they both increased the ionic conductivity by functionalizing with QA groups and improved chemical stability by using crosslinkers and fillers. However, QA group insertion is invariably not ecologically friendly, and the post-functionalization approach obstructs the development of ion transport channels, which enhances ionic conductivity [44]. Furthermore, because of the cationic group degradation brought on by the mechanisms mentioned above, the low ionic conductivity and poor chemical stability at high pH need further improvement to be used as AEM in AEMFCs.

Based on this, among other modifications, ILs have gained significant interest due to their properties, such as wide liquid range, low vapor pressure, and a perspective to increase ionic conductivity [45]. In addition, advancements have been made in applying AEMFCs: by introducing ILs to AEM, ILs may act as the "active sites" and speed up the conductivity of $OH^-$ ions [46]. Wang et al. [44] proposed a composite PVA-based AEM modified with geminal-

imidazolium-type ILs ([DimL]OH). The cross-linking action of GA trapped prepared ILs ([DimL][OH]) in the membrane structure as dopants. Adding ILs increased ionic conductivity: AEM prepared with a ratio of 1:2.5 of PVA to [DimL][OH] produced the highest conductivity of 58 mS/cm at 70 °C. After immersing for 240 hours in a 1M KOH solution, only a 4.6 % drop in $OH^-$ conductivity was observed; even in a 6M KOH solution, after 240 hours of immersion, only a 13.1 % decline was observed, demonstrating good alkaline stability [44].

Nevertheless, the green character of ILs has often been challenged due to their relatively high toxicity and poor sustainability, requiring costly and difficult preparation [45]. DESs could be an environmentally friendly alternative to ILs and be used instead of them because they have similar physicochemical characteristics. Recently, DESs have become a viable substitute electrolyte for PEMFCs because of their unique characteristics and perspective advantages [47].

Thus, PVA could be utilized as the primary polymer backbone, crosslinked with GA, and DESs could be introduced into the polymer matrix fabricated by the electrospinning method for better performance, potentially increasing ionic conductivity, chemical and mechanical stability.

## 2.3 Deep eutectic solvents and their potential for the research

### 2.3.1 ILs and DESs: similarities and differences

DESs act similarly to ILs and were introduced in recent years as an alternative to them to overcome such drawbacks of ILs and have been used in various applications such as solubility of metal oxides [48], water absorption [49], biocatalysis [50], electrochemistry [47] and many others.

ILs are molten salts with distinct anions and cations, whereas DESs are eutectic mixtures of Lewis or Brønsted acids and bases that have several cationic and anionic species, which is the primary distinction between DESs and ILs [51]. Although DES and ILs have similar physical characteristics, such as excellent thermal and chemical stability, minimal volatility, nonflammability, and adjustable viscosity, DES is less expensive to produce, biodegradable, and non-toxic. Using inexpensive and renewable chemicals as source materials is primarily the reason. In addition, DES does not require post-synthesis purification because its synthesis is a mixing process. Only the purity of the individual parts determines their purity [52]. These characteristics make DES an effective alternative for ILs. However, DES still has several drawbacks, such as high viscosity and, in some cases, it can even be solid at room temperature [52].

### 2.3.2 Fundamentals of DESs

The concept of DESs was predicated on the assumption that a eutectic mixture may form and take on physical and chemical characteristics distinct from those of the individual compounds that form the eutectic mixture [53]. QA salt, for example, ChCl, and HBDs, for instance, carboxylic acids, combine to form a DES as a result of hydrogen bonding, and the complexation between the salt and HBD, the mixture's melting point drops, resulting in the formation of a liquid as shown in Figure 2.2 [54]. Regarding the experiment, most DESs documented in the literature have a melting temperature below 100 $^{o}$C. A phenomenon like this happens when two chemicals with differing molecular sizes come together [55].

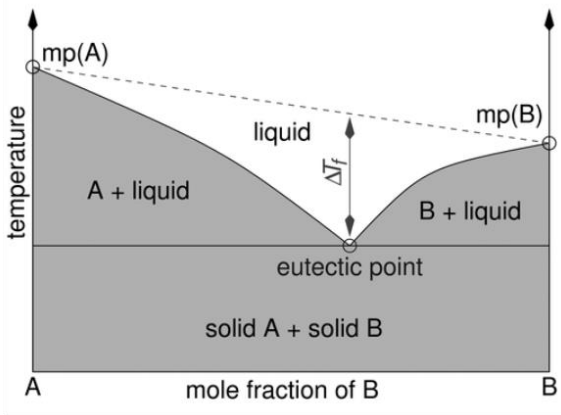


Figure 2.2 The scheme of a phase diagram demonstrated the formation of a eutectic point by mixing two components [51].

Numerous studies have demonstrated the most significant aspect of DESs is the possibility of changing their chemical and physical properties by adjusting the molar ratio of HBA to HBD [56].

Figure 2.3 illustrates a few of the frequently used HBAs and HBDs reported in the literature [57].

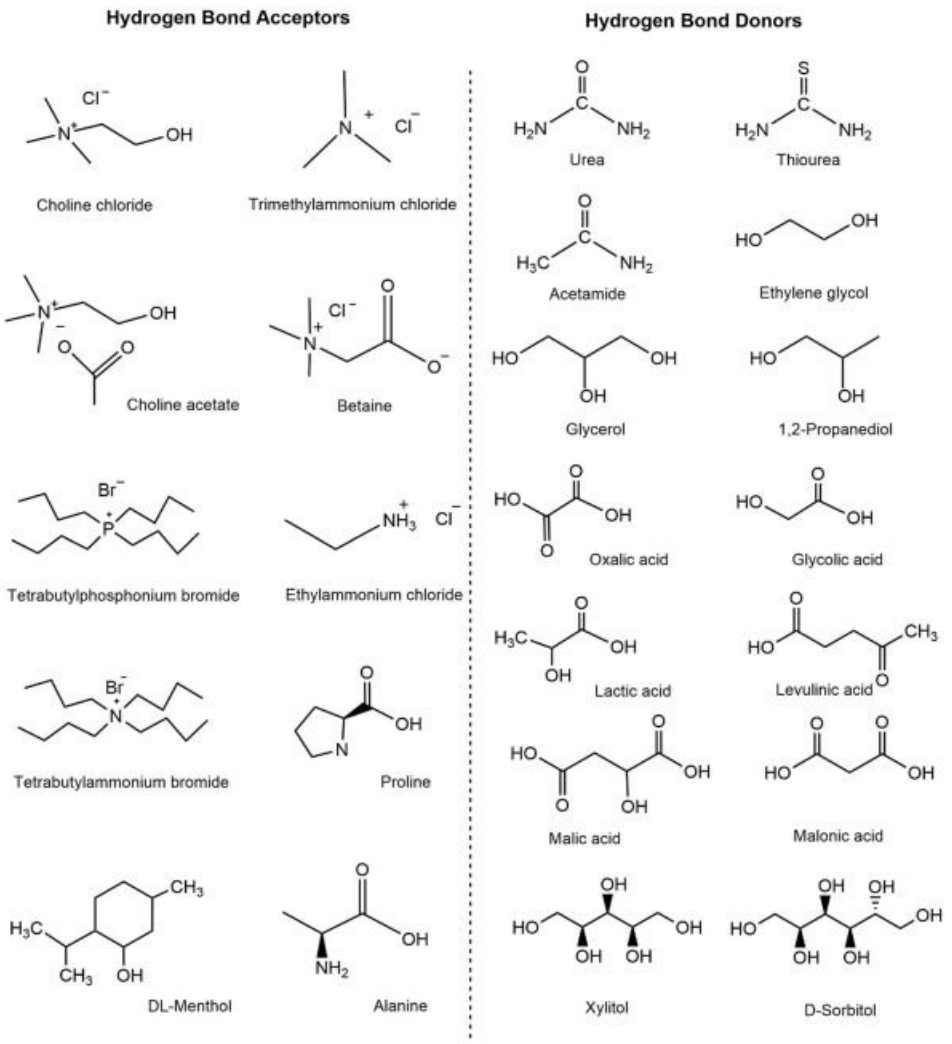


Figure 2.3 HBAs and HBDs for DES preparation [57].

The type of element compounds plays a crucial role in classification of DES; it is commonly divided into four type groups, as Table 2.2 demonstrates [51]. For instance, as a corresponding kind to imidazolium salt/metal halide systems, DESs based on QA salts and metal halides (MClx) (type I) are acknowledged. DESs containing ChCl and hydrated metal halides ($MCl_x \bullet yH_2O$) are classified as type II. Hydrated metal salts are an excellent choice for large-scale applications due to their low cost and inherent resistance to moisture and air. ChCl and HBDs combine to generate type III DESs, which are desirable because they can solvate various transition metal species, including oxides and chlorides. At room temperature, type IV DESs can incorporate transition metals into eutectics [58].

Table 2.2 Classifications of DESs [51]

| DES type | Formula | Terms |
|---|---|---|
| I | $Cat^+ X^- zMCl_x$ | M = Zn, In, Al, Fe, Sn, Ga |
| II | $Cat^+ X^- zMCl_x \bullet yH_2O$ | M = Co, Cu, Cr, Fe, Ni |
| III | $Cat^+ X^- zRZ$ | Z = COOH, $CONH_2$, OH |
| IV | $MCl_x + RZ = MCl_{x-1} + \bullet RZ + MCl_{x+1}^-$ | M = Al, Zn<br>Z = $CONH_2$, OH |

Since type III DESs are inexpensive, non-toxic, and biodegradable, they are perhaps the most researched [59]. For instance, a widely used DES can be prepared in a molar ratio 1:2 by mixing ChCl as HBA and EG as HBD. Abbott et al. first attempted to investigate this kind of DES in 2007 [60]. Biodegradable, comparatively non-toxic, and inexpensive, ChCl and EG are produced on an industrial basis [61]. Thus, they can be used as raw materials for DES preparation and further impregnation into polymer membranes.

### 2.3.3 Application of DESs in the modification of polymer electrolyte membranes

The interaction between the polymer and DESs in a polymer membrane can lead to the following options [62]:

1. application of DES just as a solvent;

2. either HBA or HBD as a DES component could be involved in the polymerization process;

3. DES might cause substantial alterations in polymers' morphological, structural, and surface characteristics.

Here, the use of DESs and their composition needs to be carefully considered to precisely adjust the characteristics of the membrane that allow the target molecules to pass through.

In addition, QA salts consist of the above-mentioned QA groups, which could play the role of ion-functionalized charge groups and be attracted physically to the polymer backbone without any quaternization, followed by a rise in the ionic conductivity. According to Shahabi et al. [63], one of their main contributions is the enhanced water movement that DESs provide after being integrated into membranes. Based on this, there is a possibility that DESs could, together with water, transport hydroxide ions. However, due to DESs' sensitivity to high water content, their

hydrogen bond interactions can be destroyed by water. Therefore, the absorption approach is the only viable method of doping them into the polymer matrix. DES characteristics may benefit from a low water content. A suitable DES should, for this purpose, have the proper viscosity and affinity to be absorbed by the polymer matrix through straightforward immersion of the polymer in the DES [47].

The innovative DES applications in polymer electrolytes aimed to increase the membranes' electrical conductivity. Using electrospinning, Rahman et al. [64] created PVA-based polymer electrolyte in 2016. The obtained nanofibrous membranes were soaked in DESs synthesized by mixing N, N-diethylethanolammonium chloride (HBA) and EG (HBD). This was further investigated since it was proved that DES' electrical conductivity varied based on the molar ratio of DES components. As a result, the obtained membranes showed remarkable electrical conductivity from $2.78 \times 10^{-6}$ to $2.27 \times 10^{-2}$ S/cm after being soaked in DESs at a molar ratio of 1:2 (HBA:HBD). Based on the results of this study, the scientists proposed that these membranes would be suitable options for particular uses in energy storage, sensors, batteries, and other areas [64]. Also, there is a possibility to investigate ionic properties by increasing the ionic conductivity of polymer electrolyte/membrane based on the PVA polymer after adding DES as a dopant due to the potential to form void spaces as conducting networks for ion conduction.

Moreover, Mano et al. [65] developed a method that encapsulates NADES from ChCl/CA in PVA nanofibers prepared by electrospinning for biomedical applications. The NADES was found to be encapsulated in the fibers by TEM, and TGA verified this finding. This work demonstrated that functionalized fibers with NADES may be fabricated by electrospinning [65]. Also, new prospects are open to implementing this method for AEMFC applications.

Much research is going on to investigate the effect of DESs on proton conductivity, specifically to achieve its increase for PEMFCs. For example, ChCl/urea (1:2) DES added to chitosan/carboxymethyl cellulose blend membranes significantly improved their proton conductivity, according to research by Wong et al. [66] under enhanced proton conduction membranes. Composite membranes, consisting of DES and 50 wt.% of CS demonstrated maximum conductivity of protons of $1.57 \times 10^{-2}$ S/cm, which was similar to commercial one (Nafion-117) of about $8.6 \times 10^{-2}$ S/cm.

Also, DES was investigated as an electrolyte for PEM modification by Karimi et al. [47] to check the effect of water on the DES-supported PEM performance. As a result, superconducting

characteristics were demonstrated by the fabricated Nafion/DES composite membrane due to the Grotthuss-like mechanism for proton conduction [47]. Thus, there is a perspective for investigating the effect of DES on AEM performance for AFC applications.

This research will investigate the effect of DES as a component of anion AEM, proposing that there will be an attraction between the polymer backbone and DES. As a result, it is expected to improve ionic conductivity, chemical and mechanical stability. Furthermore, despite several articles that have studied ion exchange membranes, mainly for PEMs, research has not yet been conducted on the DES-supported AEM for AFC application. Hence, a novel high-performance DES-supported AEM for AFCs is expected to be designed and developed by this research.

# Chapter 3 – Methodology

## 3.1 Fabrication of PVA-based fibers

### 3.1.1 Preparation of PVA solution

Overall, the PVA polymer-based nanofiber mat was fabricated using an electrospinning machine (Ne200 NanoSpinner, Inovenso). Firstly, the work that presented the most suitable PVA composite with DES suggested that the optimal concentration of the PVA solution dissolved in DI water should be 10 wt.% [64]. By heating DI water (9 g) to 90 °C in a 20 ml glass beaker equipped with a magnetic stirrer, then gradually and partially adding 1 g of PVA granulated powder (MW: 146000-186000, 87-89 % hydrolyzed) and 1-2 droplets of surfactant Triton X-100 while vigorously stirring the solution using a stirring speed of 350 rpm and temperature of 80 °C for 12 hours until all of the PVA granules were dissolved and a homogeneous transparent 10 wt.% PVA solution was obtained. The solution was then cooled to room temperature and injected into a syringe with a tip.

### 3.1.2 Electrospinning procedure

The concepts of fiber fabrication via electrospinning are explained in more detail in *1.3 Methodologies and Techniques*, where it is stated that external parameters, such as flow rate, voltage, etc., should be controlled to obtain threads with the desired thickness and quality. In this experiment, a 10 ml plastic syringe with a metallic nozzle tip at the top was filled with 4.5 ml of PVA solution and fed into the electrospinning machine to inject the solution. A drum collector wrapped in aluminum foil was used to collect fibers. Electrospinning parameters, such as flow rate, applied voltage, and nozzle-to-collector distance, were optimized and presented in Table 3.1. The electrospinning time can be varied to adjust the film's thickness.

Table 3.1 Electrospinning operating parameters

| Sample | Flow rate, ml/hr | Applied voltage, kV | Nozzle-to-collector distanc, cm | Speed of drum rotation, rpm |
|---|---|---|---|---|
| 10 wt.% PVA solution | 0.8 | 19.5 | 13 | 100 |

After obtaining nanofibers, heat treatment was conducted in the vacuum oven at 60 °C for 12 hours to remove the remaining solvent.

### 3.2 Cross-linking of pristine PVA material

While PVA is a hydrophilic polymer, its aqueous solubility limits its direct applicability. PVA chains can be crosslinked chemically to provide endurance and stability to designed materials, thereby mitigating this drawback [67]. Further improvements were performed to the obtained PVA fibers to develop crosslinked membranes. According to the literature, crosslinking the PVA fibers with GA could be a possible solution [41], [42], [44] (as mentioned in Chapter 2). Thus, the crosslinking agent was obtained by diluting GA in ethanol and adding 5M sulfuric acid $H_2SO_4$ to regulate the pH to 3, varying concentration from 4 to 8 wt.% of GA. The crosslinked membranes were prepared using the solution method stated in [68] and adapted to the material. Each dry pristine PVA membrane was submerged in the cross-linking agent for the cross-linking reaction for a different amount of time, ranging from 1 to 2 days at room temperature. The obtained crosslinked membranes were named according to the concentration of cross-linking agent used, which ranged from 4 to 8 wt.%, as PVA4, PVA6, and PVA8, respectively. As a result, a lower cross-linking time of less than 2 days was unfavorable, and the membranes shrunk. Afterward, to remove excess GA, the crosslinked membranes were washed with DI water and dried for 12 hours at 60 ºC in a vacuum oven. The effect of GA concentration is considered in Chapter 4. The cross-linking reaction between PVA and GA forming the covalent bonds is demonstrated in Figure 3.1 [69].

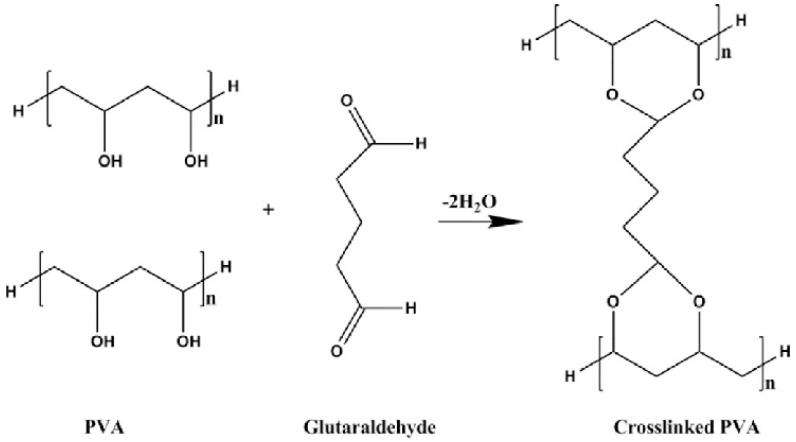


Figure 3.1 Cross-linking reaction between PVA and GA [69].

## 3.3 Preparation of DES-supported PVA-based membranes

### 3.3.1 Preparation of DESs

ChCl and EG were combined in various molar ratios to form the DES solutions, which resulted in the synthesis of four different DESs. For instance, 0.1 mole of ChCl and 0.1 mole of EG were used to prepare the DES1 solution. In order to ensure the mixture was homogeneous, two components were mixed continuously for 12 hours at 45 °C. Similarly, the moles of EG used to generate the remaining DES solutions were varied to 0.2, 0.3, and 0.4 for DES2 through DES4, respectively.

The formation of a hydrogen bond between ChCl as HBA and EG as HBD is shown in Figure 3.2 [70].

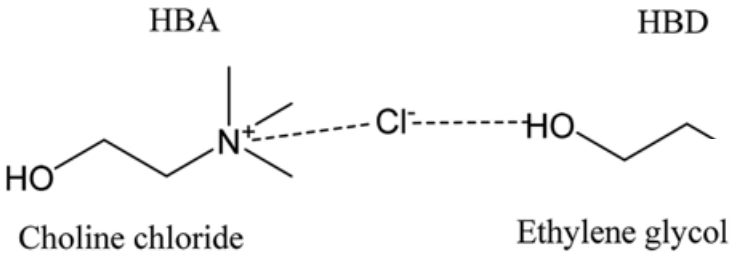


Figure 3.2 Hydrogen bond formation between ChCl and EG [70].

### 3.3.2 Soaking of crosslinked PVA membrane in DES

Crosslinked PVA membranes were immersed in DES in the Petri dishes for 24 hours. Then, when the immersion was finished, silica gel and soaked membranes were placed inside the desiccator. They were left within it for five days to dry thoroughly and then characterized. The obtained DES-supported composite AEMs were named according to the concentration of the cross-linking agent used, which ranged from 4 to 8 wt.%, and the chosen molar ratio of DES, such as DES3@PVA4, DES3@PVA6, and DES3@PVA8, respectively.

## 3.4 AEM characterization

To verify the accuracy of the data, triplicates of each type of AEMs were tested for each test.

### 3.4.1 Physical and chemical properties

Functional groups in the membranes and the interactions between various constituents were observed using Fourier transform infrared spectroscope (FTIR, Thermo Fisher Scientific Nicolet iS10 FT-IR Spectrometer). A transmission mode with a wavenumber range of 4000-500 $cm^{-1}$ and 32 scans per sample was used. The surface morphology and structure of obtained AEMs were examined by scanning electron microscope (SEM, EDX ZEISS Crossbeam 540) at magnifications of x500 and x5000. SEM samples were preliminarily coated with gold using an automatic sputter coater (Q150T) to make them more conductive. The thermogravimetric analyzer (TGA, STA 6000, Perkin Elmer) was used to evaluate the thermal stability of AEMs and to determine their composition. The measurements were conducted at a rate of 10 °C $min^{-1}$ under an inert (dry nitrogen) atmosphere at 30 to 650 °C. CHNS elemental analyzer (Elemental Vario micro cube) was used to conduct elemental analysis at 1147 ºC, with oxygen and helium flowing at 20 ml/min and 180 ml/min, respectively. Mainly to detect nitrogen content coming from DES in the obtained AEMs.

### 3.4.2 Water uptake and swelling ratio

Water content, degree of hydration, and swelling of AEM also significantly impact its performance. AEMs were punched with a disc-punching machine to get a circle-like shape (D = 19 mm) and dried until consistent weights were achieved. The weight ($M_{dry}$) and diameter ($D_{dry}$) of the AEMs were measured before the immersion. They were then soaked for 24 hours in a 1M aqueous potassium hydroxide (KOH) solution and rinsed with DI water under ambient conditions. Following the immersion procedure, the weight ($M_{wet}$) and diameter ($D_{wet}$) of the fully hydrated AEMs were immediately measured after the remaining liquid on the membrane surface was carefully removed. WU and SR of DES-supported AEMs were determined using Equations (3.1) and (3.2), respectively [42]:

$$WU = \frac{M_{wet} - M_{dry}}{M_{dry}} \times 100\ \% \tag{3.1}$$

$$SR = \frac{D_{wet} - D_{dry}}{D_{dry}} \times 100\ \% \tag{3.2}$$

where $M_{wet}$ and $D_{wet}$ are weight and diameter (length) of the moist membrane, while $M_{dry}$ and $D_{dry}$ refer to the weight and diameter (length) of the membrane dried before the immersion, respectively.

### 3.4.3 Ionic conductivity

The EIS of a potentiostat/galvanostat (Metrohm Autolab) was used to determine the membrane's ionic conductivity from $10^6$ to 1 Hz of frequency and 100 mA of current. The measurements were done at different temperatures ranging from 25 to 60 $^oC$. Before starting EIS, AEMs in spherical discs (D = 19 mm) were placed in 1M KOH solution for 24 hours to replace $Cl^-$ with $OH^-$ form before ionic conductivity testing and rinsed with DI water to remove potassium carbonates. Their thickness was measured and used for the calculation of ionic conductivity. Ready AEMs were placed between two SS blocking electrodes in a coin-type cell for the test as demonstrated in Figure 3.3.

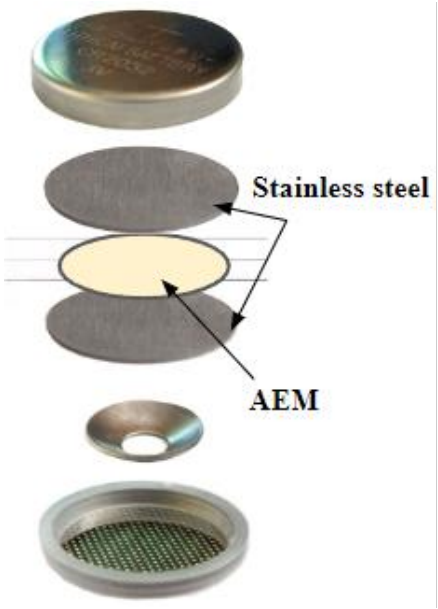


Figure 3.3 The scheme of the cell with the AEM.

Nyquist plot was utilized to evaluate bulk resistivity and calculate the ionic conductivity. Calculations were done according to Equation (3.3) [71]:

$$\sigma = \frac{h}{R\ x\ S} \tag{3.3}$$

where, $\sigma$ – ionic conductivity (mS/cm), h – thickness of the membrane (cm), R – bulk resistivity of the membrane (Ω), and S – is cross-sectional area of the membrane ($cm^2$), $S = \frac{\pi \times D^2}{4}$.

### 3.4.4 Mechanical properties

Tensile test measurements were conducted by EUTM equipment (WDW-3 Jinan HST Group Co.) to examine the mechanical characteristics of the obtained AEMs. All the membranes were selected with similar dimensions and thicknesses. After fully hydrated, the membranes were cut into 20 × 50 mm pieces with a 20 mm gap between clampings with the elongation rate of 10 mm/min. The tensile test was performed under ambient conditions. Plotting of the stress-strain curves followed.

# Chapter 4 – Results & Discussion

## 4.1 DES content

### 4.1.1 Selection of suitable molar ratio for DES preparation

Four molar ratios for DES preparation, described in detail in sub-chapter *3.3.1 Preparation of DESs* named DES1-DES4, were regarded as the most appropriate ones to meet the AEM requirements. To select one of them and confirm the presence of functional groups originated from ChCl and EG, DES1-DES4 were evaluated by FTIR. FTIR spectra for ChCl, EG, and DESs at different molar ratios (DES1-DES4) are demonstrated in Figure 4.1.

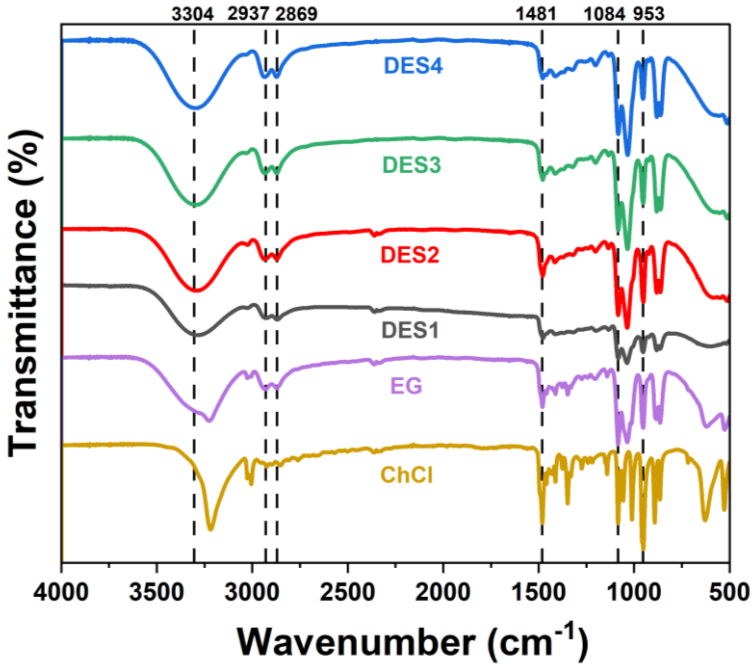


Figure 4.1 FTIR spectra for ChCl, EG, and DESs at different molar ratios.

In the spectra of DES1-DES4, a wide absorption peak of $OH^-$ stretching was noticed at around 3304 $cm^{-1}$. Due to hydrogen bonding, it was shifted to the left from the position of the ChCl peak. The results of DES preparation based on ChCl and EG, available in this work [72], stated the appearance of crucial peaks from characteristic salt (ChCl) and EG in the DES1-DES4 spectra. These are visible two peaks of $CH_2$ asymmetric and symmetric stretching at 2937 and 2869 $cm^{-1}$, respectively, originating from EG, and a peak at 953 $cm^{-1}$ of QA group $NR_4^+$ stretching originating

from ChCl, where R=$CH_3$. DESs also exhibited vibrational bands at 1481 $cm^{-1}$ to the $CH_2$ bending of an alkyl group and 1084 $cm^{-1}$ to C-O stretching [72]. Overall, the intensity of DES increases with the amount of EG due to the hydrogen bonding and the number of hydrogen bonds formed. Therefore, the spectra of DESs look almost the same visually as EG spectrum. These results indicated the successful preparation of ChCl-EG DES.

Nevertheless, observed physically, DES1 (1:1 ChCl to EG molar ratio) turned into a turbid solution as the content of ChCl and EG achieved their saturation level. DES2 (1:2 ChCl to EG molar ratio) was entirely mixed, initially creating a transparent solution, but after five days, the crystallization of ChCl was observed. Starting from DES3 (1:3 ChCl to EG molar ratio), the solution sustained the homogeneity and transparency for a long time. The photography of DESs prepared at different molar ratios after five days is provided in Figure 4.2.


Figure 4.2 Photography of DESs prepared at different molar ratios.

Compared with the most investigated DES2, DES3 revealed higher homogeneity and transparency, which could improve ionic conductivity better than DES1 and DES2 due to its lower viscosity. Moreover, DES3 is more similar in composition to DES2 than DES4; hence, DES4 was not considered. In addition, there is no significant difference among DES1-DES4, as illustrated in Figure 4.1, where all major peaks from ChCl and EG exist at all considered ratios. Since one of the goals was adding DES into a PVA-based nanofiber mat to obtain AEM, preference was given to DES3 as an additive. After that, before soaking the fibers in DES, they should be crosslinked first.

## 4.2 Modification of PVA fibers by cross-linking

Due to their high hydrophilicity, pristine PVA fibers were crosslinked with GA solution of different concentrations. As a result, the crosslinked PVA membranes remained stable in aqueous potassium hydroxide solution, confirming their stability after cross-linking.

### 4.2.1 Surface characterization of pristine and crosslinked PVA membranes

The surface morphology of pristine and crosslinked PVA materials were analyzed by SEM and illustrated in Figure 4.3.

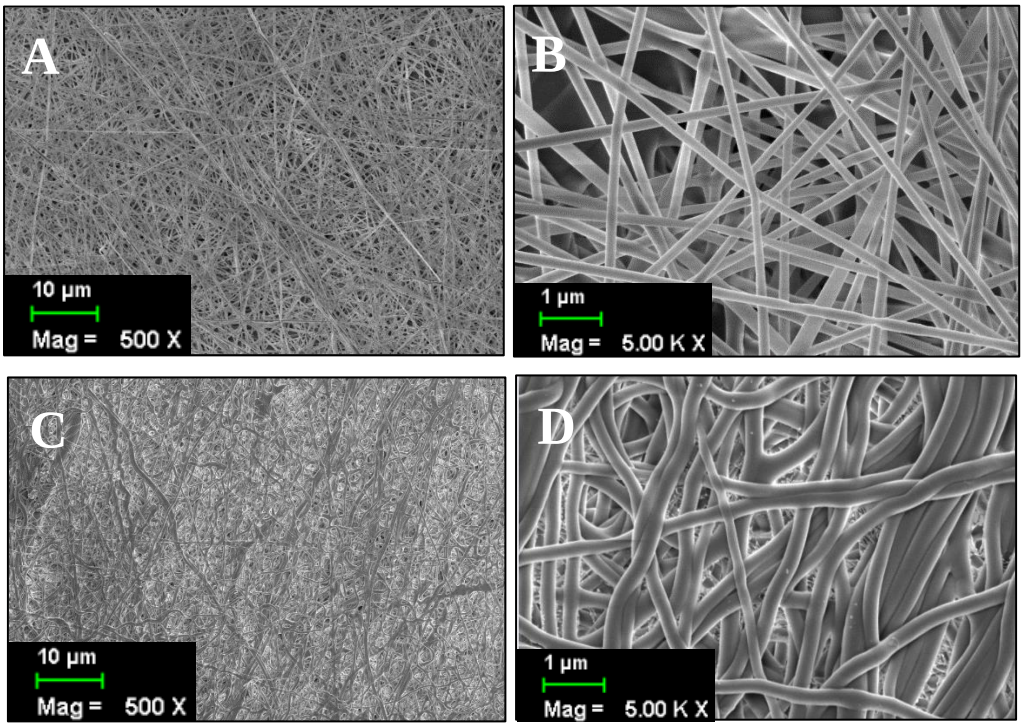


Figure 4.3 SEM images of the top views of (A,B) pristine PVA and (C,D) PVA4 at magnification 500x and 5000x, respectively.

Pristine PVA fibers have sustained a uniform diameter distribution ranging from 400-500 nm, randomly arranged (Figure 4.3 A,B). As seen in Figures 4.3 A and B, the morphology of pristine PVA fibers is homogenous and smooth, with no beads or entanglements and a large surface area. It was expected that impregnating PVA fibers with GA would produce a more robust and stiff material with a denser structure by cross-linking them. After cross-linking, membranes appeared less porous, with fibers changing their shape from straight to relaxed, slightly enlarged

in diameter, and merged as entanglements in some areas, as demonstrated in Figure 4.3 C,D. So, notable difference between the obtained SEM images of pristine PVA and the crosslinked one can be observed, which proves the cross-linking effect. Still, the chemical interaction between PVA and GA was checked using FTIR analysis for full confirmation.

### 4.2.2 FTIR analysis of pristine and crosslinked materials

FTIR spectra of pristine PVA, crosslinking agent, and PVA membranes crosslinked with GA solution of different concentrations are shown in Figure 4.4 A.

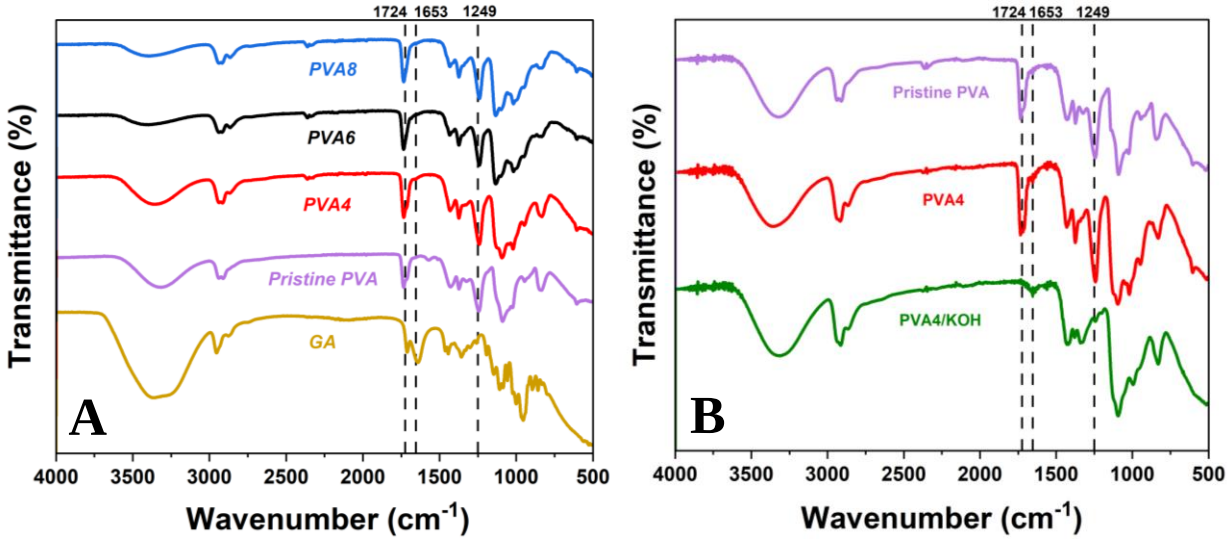


Figure 4.4 FTIR spectra: (A) for pristine PVA, PVA4-PVA8 and (B) for pristine PVA, PVA4, and PVA4 after immersion in 1M KOH.

According to Figure 4.4 A, there is no difference among the spectra of all crosslinked PVA membranes (PVA4-PVA8), and they revealed a characteristic peak with the lower intensity at 1653 $cm^{-1}$ of C=O stretching from GA because this peak is not visible in the pristine PVA spectrum [73]. The appearance of this peak confirmed that cross-linking has successfully occurred within PVA.

FTIR spectra of pristine PVA, crosslinked PVA membrane (PVA4), and after its immersion in 1M potassium hydroxide solution for 24 hours are shown in Figure 4.4 B. Since there is no difference among the spectra of all crosslinked PVA membranes (PVA4-PVA8), PVA4 was chosen to be immersed in potassium hydroxide for 24 hours following the AEM working

requirements for AFC and analyzed by FTIR. In the red-colored spectrum of PVA4 immersed in KOH from Figure 4.4 B, the disappearance of the C=O stretching peak at 1724 $cm^{-1}$ and C-O-C vibrational peak at 1249 $cm^{-1}$ from PVA was observed due to hydrolysis of the non-reacted acetyl groups from pristine PVA, precisely from polyvinyl acetate by $OH^-$ groups of KOH [74]. Moreover, the C=O peak at 1653 $cm^{-1}$ from GA was preserved with the cross-linking effect after immersion in KOH. Based on the SEM and FTIR results, the obtained crosslinked PVA membranes were stable in aqueous and alkaline medium and can be further impregnated with DES.

## 4.3 Composite membrane: integration of crosslinked PVA-based membranes and DES

### 4.3.1 Surface characterization of composite membrane and after its immersion in potassium hydroxide solution

SEM images of PVA-based AEM reinforced with DES and immersed in potassium hydroxide solution are illustrated in Figure 4.5.

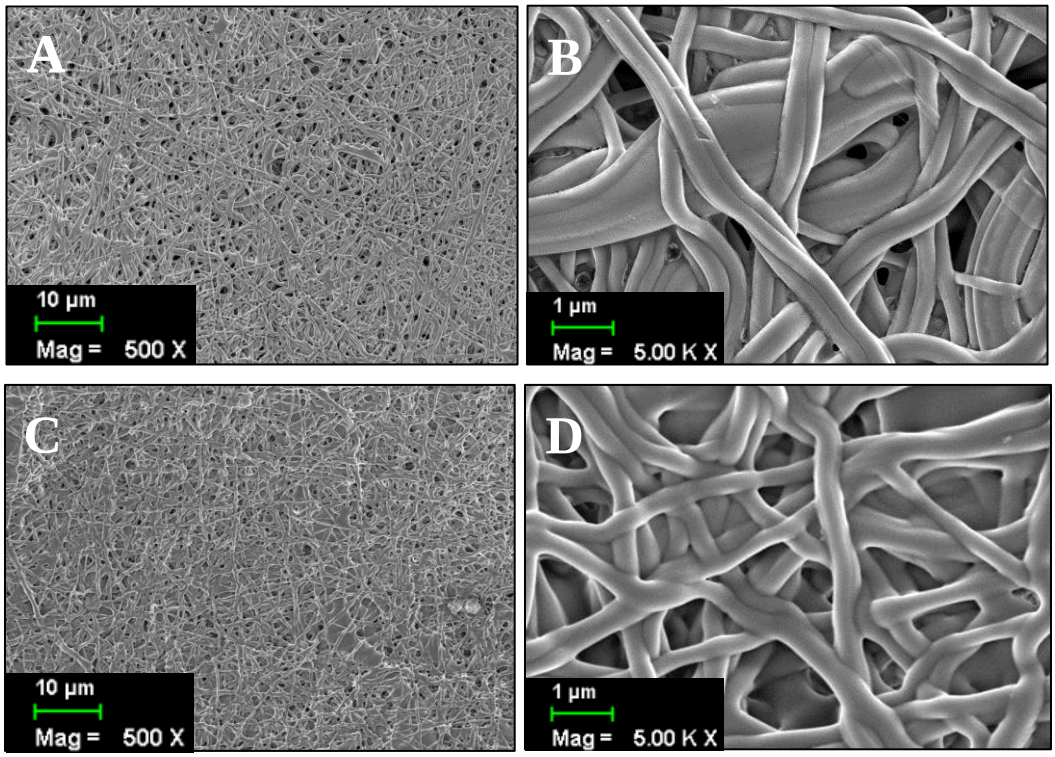


Figure 4.5 SEM images of the top views of (A,B) DES3@PVA4 and (C,D) DES3@PVA4 after immersion in 1M KOH at magnification 500x and 5000x, respectively.

In Figure 4.3 it was observed that the PVA fibers overlap and create a three-dimensional networked area with linked pores and voids in between. An arrangement like this facilitates the straightforward penetration of DES into the membrane structure and prevents leaks, which leads to high mechanical characteristics and ionic conductivity. So, in Figure 4.5 A,B it can be seen that DES occupied most of the void areas in the PVA-based nanofibrous membrane, resulting in DES-supported composite AEM. Also, to check its stability, AEM was immersed in a 1M KOH solution for 24 hours. However, as mentioned above, potassium carbonate formation is possible, so the surface of the membrane was rinsed slightly with DI water. From Figures 4.5 C and D, the absence of particles was observed. Thus, all the potassium carbonates were washed with water. Moreover, there was no degradation, the nanofibrous structure was preserved, and pores were still present.

### 4.3.2 FTIR analysis of pristine, crosslinked, and composite membranes

As was mentioned in the sub-chapter *4.2.2 FTIR analysis of pristine and crosslinked materials*, there is no difference among PVA4-PVA8 spectra (Figure 4.4 A). Thus, for FTIR analysis of all composite membranes (DES3@PVA), the preference was given to DES3@PVA4. FTIR spectra for pristine PVA, crosslinked PVA membrane in 4 wt.% GA solution (PVA4), DES3 (1:3 ChCl to EG molar ratio), the product after the soaking in DES3 (DES3@PVA4) are demonstrated in Figure 4.6.

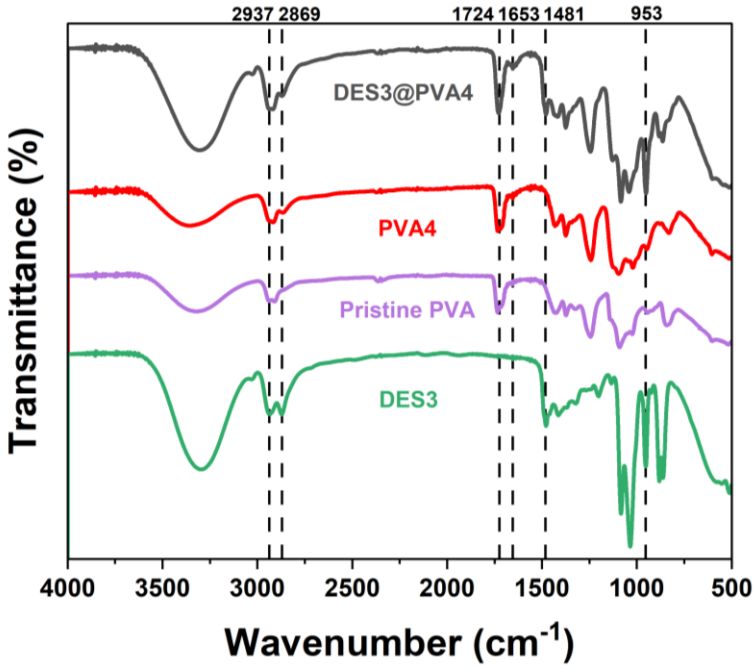


Figure 4.6 FTIR spectra of pristine PVA, PVA4, DES3, and DES3@PVA4.

The spectrum modified with DES composite AEM has the carbonyl stretching frequency of C=O from PVA, which was observed at 1724 $cm^{-1}$ [74]. The presence of DES in composite membranes was confirmed above by two visible peaks of $CH_2$ asymmetric and symmetric stretching at 2937 and 2869 $cm^{-1}$ originating from EG, respectively, and a peak at 953 $cm^{-1}$ of QA group $NR_4^+$ stretching originated from ChCl, where R=$CH_3$ [72]. Moreover, comparing all spectra in Figure 4.6, the changes in the peak at 1481 $cm^{-1}$ after introducing DES were noticeable. They corresponded to $CH_2$ bending, the most recognizable group in all ChCl-based DESs [75]. Based on the FTIR results, DES and PVA, particularly their functional groups, were examined and compared in the DES-supported composite AEM; no new peak was identified in the spectra. Therefore, it is suggested that due to hydrogen bonding interactions, there is a physical absorption of DES within the PVA membrane, and DES is not chemically reacted to PVA. Furthermore, by combining this information with weight loss curves obtained by TGA analysis, it is possible to indicate the composition of composite membranes qualitatively.

### 4.3.3 TGA analysis of pristine, crosslinked, and composite membranes

TGA analysis was performed to qualitatively identify the composition of DES-supported composite membranes and evaluate their thermal stability compared to pristine and crosslinked unmodified membranes. The results of the TGA analysis of pristine PVA, crosslinked PVA membranes at different concentrations of GA, and DES-supported composite AEMs are presented in Figure 4.7.

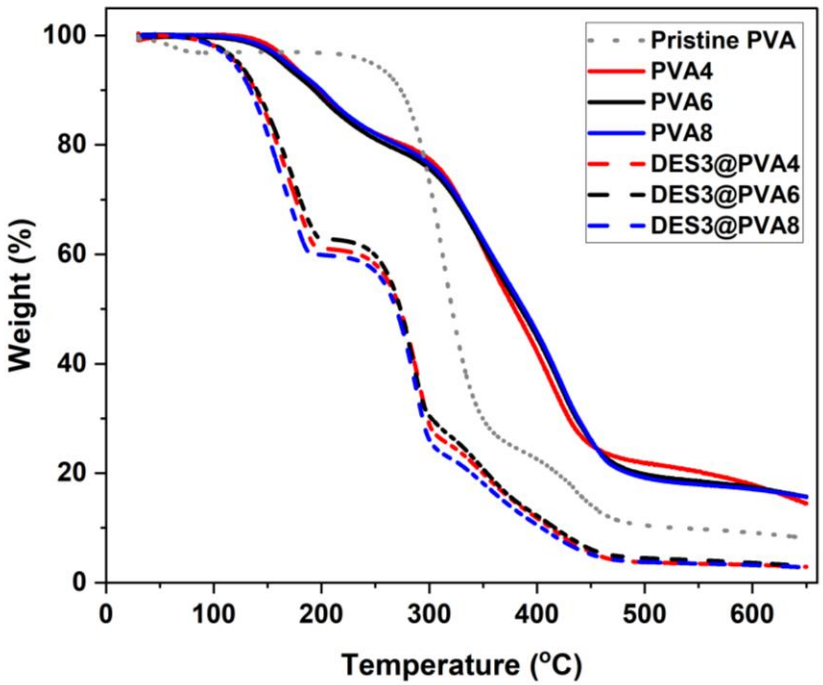


Figure 4.7 TG curves of pristine PVA, crosslinked PVA membranes with GA solution of different concentrations, and composite AEMs.

Initial weight loss was detected in the TG curve of pristine PVA from 30 to 100 °C. This was caused by water molecules' evaporation from AEMs and moisture absorption from the surrounding environment. The second weight loss, which occurred at a temperature range of 250–370 °C, was caused by its initial degradation. The third weight loss, which occurred at 390–475 °C is related to backbone C-C bond cleavage [41, 42]. Considering the TG curves of crosslinked samples (PVA4-PVA8), the breakage of cross-linking bonds occurred between 150 and 305 °C, starting with 305 °C, and the subsequent weight loss was associated with the degradation of PVA itself [42]. TG curves of all composite membranes (DES3@PVA) comprised of two weight loss stages, from 100 to 200 °C and 200 to 300 °C, matching EG and ChCl, respectively [75]. The weight loss curve began at about 255 °C, indicating thermal degradation of PVA [65]. Based on TGA results, the weight loss curves of DES-supported composite AEMs indicated the presence of each of their components, with weight losses from the DES components and the PVA. However, DES-supported composite AEMs have lower thermal stability than pristine and crosslinked PVA membranes. Nevertheless, they are suitable for low-temperature fuel cells due to their adequate

thermal stability. Besides this, using CHNS analysis allowed for quantitative determination of the percentage of nitrogen to confirm the presence of DES in the composite membranes.

### 4.3.4 CHNS analysis of pristine and composite membranes

The carbon, hydrogen, and nitrogen content of pristine PVA and DES-supported composite membranes were determined using a CHNS analyzer. The results are illustrated in Figure 4.8. The DES-supported composite membranes were analyzed for one month immersed in 1M KOH to check the presence of DES in the system.

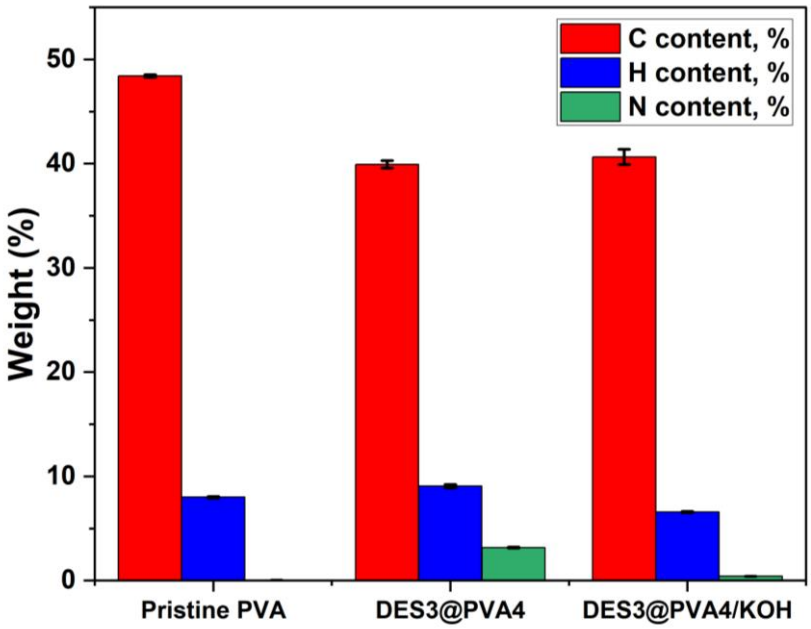


Figure 4.8 Carbon, hydrogen, and nitrogen content charts of pristine PVA, composite AEMs, and composite AEMs after immersion in 1M KOH.

In order to confirm the presence of DES in the obtained composite AEMs, the nitrogen content was investigated because ChCl contains nitrogen, and it was also confirmed by FTIR results, as shown in Figure 3.2 and Figure 4.1, respectively. According to Figure 4.8, pristine PVA membranes, as expected, did not contain nitrogen. Considering DES-supported composite AEMs, membranes had a nitrogen content of 3.16 ± 0.05 wt.%. After one month of immersion in a potassium hydroxide solution, it became 0.41 ± 0.01 wt.% in membranes. These results indicated that DES uptake by the PVA-based nanofiber matrix occurred. Even if DES escaped the system

after a long period in the potassium hydroxide solution, some amount of DES was still kept in AEM.

To summarize, FTIR, SEM, TGA, and CHNS analysis results demonstrated the successful outcome of synthesis of all DES-supported composite membranes by sustaining stability after cross-linking in an alkaline medium and the presence of DES in the membranes. Before the ionic conductivity and tensile tests of the obtained AEMs, the WU and SR tests were conducted to evaluate their water content.

### 4.3.5 Water uptake and swelling ratio of crosslinked PVA and composite membranes

As was discussed above, water must be present in AEMs to achieve a high $OH^-$ conductivity. Thus, 1M aqueous potassium hydroxide solution was chosen as a conductive aqueous medium to examine the uptake and swelling of the prepared membranes. The ionic conductivity can be increased by water clusters acting as anion transport pathways within the AEM. On the other hand, extensive membrane swelling caused by excessive WU could result in poor dimensional stability, hindering the ion-conducting performance of the membrane [76].

The WU charts of the crosslinked PVA membranes and DES-supported composite AEMs are depicted in Figure 4.9.

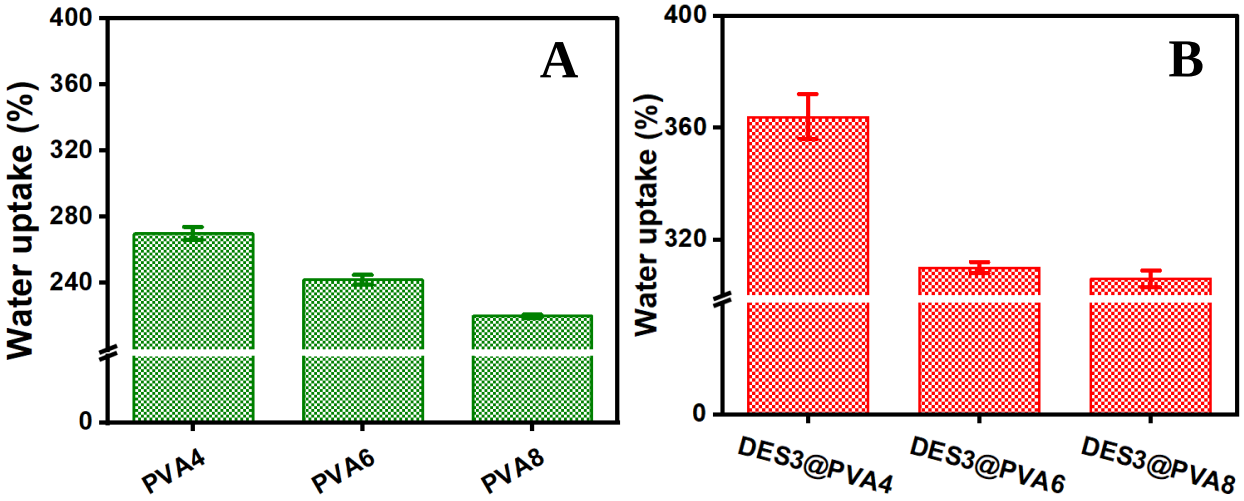


Figure 4.9 WU of (A) crosslinked PVA membranes with GA solution of different concentrations and (B) DES-supported composite AEMs.

The modification using DES as an additive to crosslinked PVA membranes was followed by elevated hydrophilicity of membranes. Consequently, the WU capability rose from 270 ± 4 %

(non-modified with DES AEM, PVA4) to 364 ± 4 % (modified AEM, DES3@PVA4). However, the WU of DES3@PVA4 decreased with the increase of GA concentration as follows to 6 wt.% and 8 wt.%, resulting in the WU values such as 310 ± 2 % (DES3@PVA6) and 306 ± 3 % (DES3@PVA8), respectively. Likewise, the result for WU of non-modified crosslinked membranes was similar to WU of modified ones.

Significant hygroscopicity of DES is expected to be attributed to the hydrophilic groups $Cl^-$ and $OH^-$ present in the molecule, which could result a rise in WU and SR [77]. Despite this, SR was measured according to the diameter (length) change between the dry and wet states of the disc-shaped membrane. No difference was observed for all the samples due to cross-linking. Based on these results, the increase in cross-linking degree resulted in a denser and more compact micro-network structure. Hence, limited space for water transport was the leading cause of the reduction of WU and the absence of swelling [76]. Thus, the SR was evaluated and equal to zero, leading to high dimensional stability or mechanical properties. Overall, modification with DES and hydrophilicity of PVA indicates that water was absorbed by the nanofiber structure (each fiber swells), followed by higher ionic conductivities while suppressing dimensional changes (bulk does not change significantly).

### 4.3.6 Ionic conductivity of composite membranes

All DES-supported composite membranes at different cross-linking degrees and with a thickness of around 100 μm were tested by impedance spectroscopy to investigate ionic conductivity from 25 to 60 $^oC$ temperatures. Before assembling the cell, it was immersed in an aqueous 1M potassium hydroxide solution for 24 hours, and the membrane surface was slightly rinsed with DI water. Figure 4.10 shows the dependence of ionic conductivities of non-modified crosslinked membrane (PVA4) and DES-supported composite AEMs (DES3@PVA) on temperature.

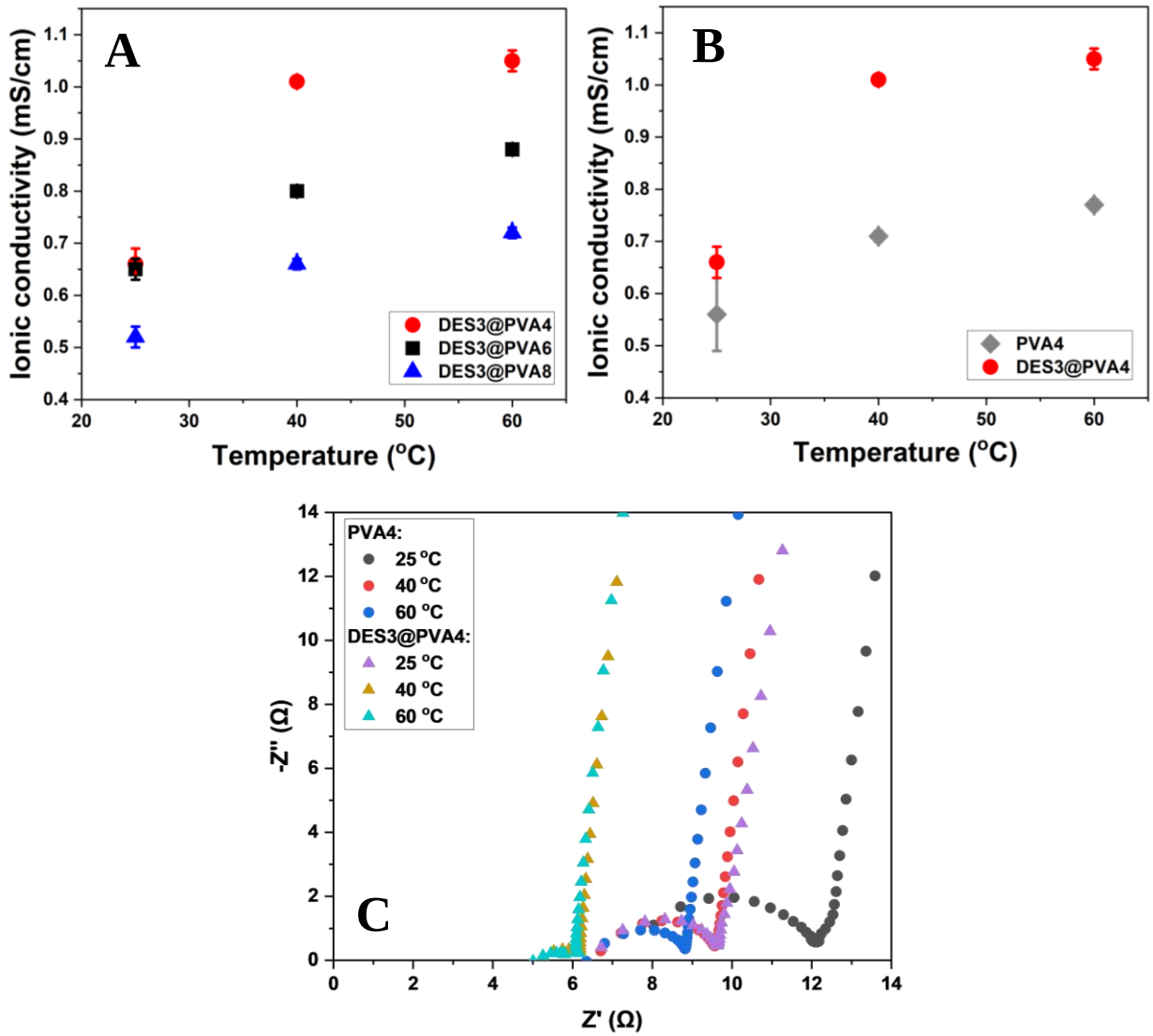


Figure 4.10 Ionic conductivity at 25, 40, and 60 °C of (A) composite AEMs (DES3@PVA), (B) PVA4, DES3@PVA4, and (C) Nyquist plots of PVA4, DES3@PVA4.

Based on Figure 4.10 A, the ionic conductivity of each composite AEM raised with temperature under the same conditions because of increased ion mobility at higher temperatures. Furthermore, higher temperature might cause the AEMs' free space to expand, which is advantageous for conducting ions [76]. Among all modified composite AEMs, the ionic conductivity varied between 0.5 and 1.1 mS/cm at lower and higher temperatures. Moreover, the ionic conductivity and WU had the same trend (Figure 4.9 B). With the increase of the concentration of cross-linking agent GA from 4 wt.% to 8 wt.%, the decrease in ionic conductivity was observed due to a higher cross-linking degree. So, the increase in the cross-linking degree

resulted in low water absorption, hence the deficit of $OH^-$ groups in the system. Since DES3@PVA4 demonstrated the highest values of ionic conductivity, such as 0.66 ± 0.03 mS/cm at room temperature, 1.01 ± 0.01 mS/cm at 40 $^oC$, and 1.05 ± 0.02 mS/cm at 60 $^oC$, thus DES3@PVA4 was compared with the non-modified one (PVA4) to evaluate the effect of DES on ionic conductivity.

Figure 4.10 B illustrates the ionic conductivities of crosslinked PVA-based membranes (PVA4) and after modification with DES (DES3@PVA4) from 25 to 60 $^oC$. It can be observed that impregnation with DES had boosted the hydroxide conductivity of the DES3@PVA4 compared to the non-modified one (PVA4). After impregnation with DES ionic conductivity has increased from 0.56 ± 0.07 to 0.66 ± 0.03 mS/cm at room temperature, from 0.71 ± 0.01 to 1.01 ± 0.01 mS/cm at 40 $^oC$, and from 0.77 ± 0.01 to 1.05 ± 0.02 mS/cm at 60 $^oC$. Based on this, a significant difference between ionic conductivity values can be observed when the temperature is raised from 25 to 40 $^oC$. However, there was a slight increase in ionic conductivity from 40 to 60 $^oC$. This might be related to the potassium hydroxide solution's evaporation start in this temperature range.

Nyquist plots of crosslinked PVA membranes (PVA4) and DES-supported composite AEMs (DES3@PVA4) generated by electrochemical impedance spectroscopy from 25 to 60 $^oC$ and the frequency of $10^6$ Hz to 1 Hz are summarized in Figure 4.10 C. Based on these plots, hydrated membranes' bulk resistances (R) were found at the interception of semicircles with the real impedance axis. This Figure demonstrated that DES3@PVA4 at 60 $^oC$ had the minimum bulk resistance and was predicted to have adequate ionic conductivity, corresponding to the data provided in Figure 4.10 B. So, DES3@PVA4 was found to be the AEM with the highest ionic conductivity, but it must also maintain the required mechanical strength to withstand pressing during cell assembly and operation [42].

### 4.3.7 Mechanical properties of crosslinked PVA and composite membranes

Assembling the cell requires careful consideration of the mechanical properties, such as tensile strength and elongation at the break of the AEMs [42]. Accordingly, the mechanical stability of crosslinked PVA and DES-supported composite AEMs at a fully hydrated state was examined in the form of the stress-strain curves shown in Figure 4.11.

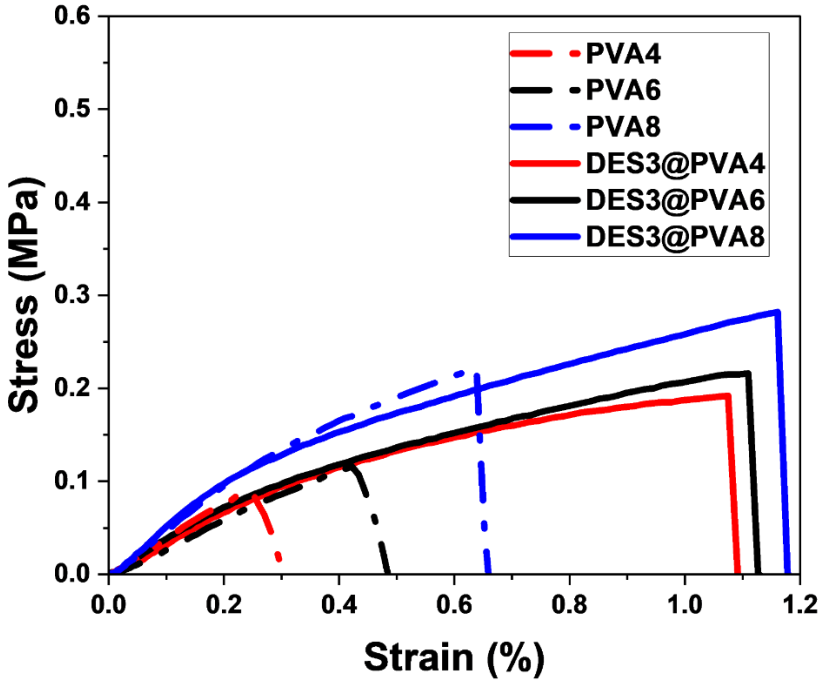


Figure 4.11 Stress-strain curves of crosslinked PVA membranes and DES-supported composite AEMs with GA solution of different concentrations.

Comparing all non-modified crosslinked PVA membranes, the improvement of mechanical properties with the increase of cross-linking degree could be observed. For instance, PVA4, the most hydrophilic of all the unmodified membranes with the greatest WU, was mechanically weaker when fully hydrated. The tensile strength and elongation at the break of PVA4 were 0.09 MPa and 0.24 %, respectively. By increasing the concentration of GA solution from 4 wt.% to 8 wt.%, the tensile strength and breaking strain were grown around 2.5 and 2.7 times, respectively.

The same trend was observed with the increase of cross-linking degree for the modified AEMs, despite the increase in both tensile strength and breaking strain not being sufficient, and all of them were practically the same. However, introducing DES to the system was followed by significantly enhancing the mechanical properties, especially elongation. For example, the tensile strength and elongation at the break of DES3@PVA4 were 0.19 MPa and 1.08 %, respectively. Therefore, the elongation at the break of DES3@PVA4 was almost 4.5 times higher than those of unmodified crosslinked PVA membranes. In conjunction with the impregnation with DES, the DES3@PVA8 exhibited the maximum tensile strength of 0.28 MPa and elongation at the break of 1.16 %. Strong interactions between the polymer matrix and DES resulted in improved mechanical

characteristics. Including DES most likely enhanced the amorphous phases of the polymer matrix, which can decrease its crystallinity. Furthermore, the presence of DES improves the formation of additional Wan der Waals forces due to the hydrogen bonding within PVA and DES, leading to a plasticizing effect confirmed by a high degree of elongation.

To sum up, the main objective of the current work was to achieve a certain level of hydroxide conductivity and mechanical stability at a controlled degree of water uptake and swelling ratio. This was achieved by fabricating PVA-based fibers by electrospinning them, cross-linking them using GA as a cross-linking agent, and further modifying the impregnation of the crosslinked PVA membrane with DES. The characterization results of crosslinked PVA membranes without modification and DES-supported composite AEMs are summarized in Table 4.1 and demonstrate the improvement after the modification.

Table 4.1 Characterization results of crosslinked PVA membranes without modification and DES-supported composite AEMs

| **Membrane** | **WU, %** | **SR, %** | **Ionic conductivity, mS/cm** | **Tensile strength, MPa** | **Elongation at break, %** |
|---|---|---|---|---|---|
| PVA4 | 270 ± 4 | 0 | 0.56 ± 0.07 (25 °C)<br>0.71 ± 0.01 (40 °C)<br>0.77 ± 0.01 (60 °C) | 0.09 | 0.24 |
| PVA6 | 242 ± 3 | 0 | - | 0.12 | 0.42 |
| PVA8 | 220 ± 1 | 0 | - | 0.22 | 0.64 |
| DES3@PVA4 | 364 ± 8 | 0 | 0.66 ± 0.03 (25 °C)<br>1.01 ± 0.01 (40 °C)<br>1.05 ± 0.02 (60 °C) | 0.19 | 1.08 |

| | | | | | |
|---|---|---|---|---|---|
| DES3@PVA6 | 310 ± 2 | 0 | 0.65 ± 0.02 (25 ºC)<br>0.80 ± 0.01 (40 ºC)<br>0.88 ± 0.01 (60 ºC) | 0.22 | 1.11 |
| DES3@PVA8 | 306 ± 3 | 0 | 0.52 ± 0.02 (25 ºC)<br>0.66 ± 0.01 (40 ºC)<br>0.72 ± 0.01 (60 ºC) | 0.28 | 1.16 |

Modified DES3@PVA membranes possess higher ionic conductivity and decent mechanical properties due to a higher elongation degree than pristine PVA membranes. Since all the modified membranes had approximately the same mechanical characteristics, which were higher than for non-modified ones, DES3@PVA4, crosslinked by GA solution at a concentration of 4 wt.%, was chosen as the most suitable membrane, characterized by the highest hydroxide conductivity among all prepared membranes.

# Conclusions

In conclusion, this research focused on acquiring highly conductive and mechanically stable DES-supported PVA-based composite AEMs for AFC applications. PVA fibers were fabricated via the electrospinning method and crosslinked using GA solution of different concentrations to achieve this target. DES3, with the molar ratio of 1:3 of ChCl and EG, respectively, was chosen as the most suitable one due to its stability, homogeneity after an extended period, and relatively low viscosity compared to other ratios corresponding to higher ionic conductivity. Then, the obtained crosslinked PVA membranes were modified by impregnation with DES, and the optimal cross-linking degree of the DES-supported composite membranes was examined. As a result, the DES-supported composite AEM named DES3@PVA4 (crosslinked with a 4 wt.% GA solution) demonstrated the highest hydroxide conductivity of 0.66 ± 0.03 and 1.05 ± 0.02 mS/cm at room temperature and 60 $^{o}$C, respectively.

Along with high ionic conductivity, the DES3@PVA4 composite membrane maintained the original nanofiber structure's potential for avoiding areal swelling. The absence of swelling also impacted the moderate water uptake (364 ± 8 %) and enhanced tensile characteristics with a tensile stress of 0.19 MPa and elongation at break of 1.08 %, particularly elongation that was adequate to maintain the membrane's integrity. Thus, since all modified DES-supported composite membranes had almost the same mechanical properties, DES3@PVA4 was revealed as the most optional and high-performance AEM. It fulfills all the AEM requirements considered for the AFC application due to the sufficient conductivity of hydroxide ions and sustains ductility.

# References

[1] R. Sood, S. Cavaliere, D. J. Jones, and J. Rozière, “Electrospun nanofibre composite polymer electrolyte fuel cell and electrolysis membranes,” *Nano Energy*, vol. 26, pp. 729–745, 2016.

[2] J. Xue, T. Wu, Y. Dai, and Y. Xia, “Electrospinning and electrospun nanofibers: Methods, materials, and applications,” *Chem. Rev.*, vol. 119, no. 8, pp. 5298–5415, 2019.

[3] T. Tamura and H. Kawakami, “Aligned electrospun nanofiber composite membranes for fuel cell electrolytes,” *Nano Lett.*, vol. 10, no. 4, pp. 1324–1328, 2010.

[4] P. J. Megía, A. J. Vizcaíno, J. A. Calles, and A. Carrero, “Hydrogen production technologies: From fossil fuels toward renewable sources. A mini review,” *Energy Fuels*, vol. 35, no. 20, pp. 16403–16415, 2021.

[5] C. Sun et al., “An efficient barrier toward vanadium crossover in redox flow batteries: The bilayer [Nafion/(WO3)x] hybrid inorganic-organic membrane,” *Electrochim. Acta*, vol. 378, no. 138133, p. 138133, 2021.

[6] I. Tikiz and I. Taymaz, “An experimental investigation of solid oxide fuel cell performance at variable operating conditions,” *Therm. Sci.*, vol. 20, no. 5, pp. 1421–1433, 2016.

[7] A. C. Bhosale, S. R. Suseendiran, R. Ramya, S. R. Choudhury, and R. Rengaswamy, “Phosphoric acid fuel cells,” in Comprehensive Renewable Energy, *Elsevier*, 2022, pp. 437–458.

[8] R. R. Contreras, J. Almarza, and L. Rincón, “Molten carbonate fuel cells: a technological perspective and review,” *Energy Sources Recovery Util. Environ. Eff.*, pp. 1–15, 2021.

[9] G. P. Panayiotou, S. A. Kalogirou, and S. A. Tassou, “PEM fuel cells for energy production in solar hydrogen systems,” *Recent Patents on Mechanical Engineeringe*, vol. 3, no. 3, pp. 226–235, 2010.

[10] D. R. Dekel, “Review of cell performance in anion exchange membrane fuel cells,” *J. Power Sources*, vol. 375, pp. 158–169, 2018.

[11] J.-H. Wee, “Applications of proton exchange membrane fuel cell systems,” *Renew. Sustain. Energy Rev.*, vol. 11, no. 8, pp. 1720–1738, 2007.

[12] H. Tang, S. Peikang, S. P. Jiang, F. Wang, and M. Pan, “A degradation study of Nafion proton exchange membrane of PEM fuel cells,” *J. Power Sources*, vol. 170, no. 1, pp. 85–92, 2007.

[13] A. Kusoglu and A. Z. Weber, “New insights into perfluorinated sulfonic-acid ionomers,” *Chem. Rev.*, vol. 117, no. 3, pp. 987–1104, 2017.

[14] W. Dai *et al.*, “A review on water balance in the membrane electrode assembly of proton exchange membrane fuel cells,” *Int. J. Hydrogen Energy*, vol. 34, no. 23, pp. 9461–9478, 2009.

[15] J. Fang, Y. Wu, Y. Zhang, M. Lyu, and J. Zhao, “Novel anion exchange membranes based on pyridinium groups and fluoroacrylate for alkaline anion exchange membrane fuel cells,” *Int. J. Hydrogen Energy*, vol. 40, no. 36, pp. 12392–12399, 2015.

[16] M. Hren, M. Božič, D. Fakin, K. S. Kleinschek, and S. Gorgieva, “Alkaline membrane fuel cells: anion exchange membranes and fuels,” *Sustain. Energy Fuels*, vol. 5, no. 3, pp. 604–637, 2021.

[17] M. Iravaninia and S. Rowshanzamir, “Polysulfone-Based Anion Exchange Membranes for Potential Application in Solid Alkaline Fuel Cells,” *J. Renew. Energy Environ*, vol. 2, pp. 59–65, 2015.

[18] G. Merle, M. Wessling, and K. Nijmeijer, “Anion exchange membranes for alkaline fuel cells: A review,” *J. Memb. Sci.*, vol. 377, no. 1–2, pp. 1–35, 2011.

[19] G. Das, J.-H. Choi, P. K. T. Nguyen, D.-J. Kim, and Y. S. Yoon, “Anion exchange membranes for fuel cell application: A review,” *Polymers (Basel)*, vol. 14, no. 6, p. 1197, 2022.

[20] J. Ran *et al.*, “Ion exchange membranes: New developments and applications,” *J. Memb. Sci.*, vol. 522, pp. 267–291, 2017.

[21] T. B. Ferriday and P. H. Middleton, “Alkaline fuel cell technology - A review,” *Int. J. Hydrogen Energy*, vol. 46, no. 35, pp. 18489–18510, 2021.

[22] C. Ding and Z. Qiao, “A review of the application of polyvinyl alcohol membranes for fuel cells,” *Ionics (Kiel)*, vol. 28, no. 1, pp. 1–13, 2022.

[23] S. Jeong, J. Lee, S. Woo, J. Seo, and B. Min, “Characterization of anion exchange membrane containing epoxy ring and C–cl bond quaternized by various Amine groups for application in fuel cells,” *Energies*, vol. 8, no. 7, pp. 7084–7099, 2015.

[24] X. Gong, G. He, X. Yan, Y. Wu, W. Chen, and X. Wu, “Electrospun nanofiber enhanced imidazolium-functionalized polysulfone composite anion exchange membranes,” *RSC Adv.*, vol. 5, no. 115, pp. 95118–95125, 2015.

[25] G. A. Arı and Z. Özcan, “A novel approach for stable anion exchange membrane: Self-assembled multilayer formation on the membrane via LbL method,” *Synth. Met.*, vol. 220, pp. 269–275, 2016.

[26] T. Zhou, B. Ao, Y. Wei, S. Chen, K. Lian, and J. Qiao, “Fabricating hydroxyl anion conducting membranes based on poly(vinyl alcohol) and bis(2-chloroethyl) ether-1,3-bis[3-(dimethylamino)propyl] urea copolymer with linear anion-exchange sites for polymer electrolyte membrane fuel cell,” *Solid State Ion.*, vol. 308, pp. 112–120, 2017.

[27] J. Zhang, G. Jiang, and J. Shi, “Vinyl Alcohol)/Sulfosuccinic Acid (PVA/SSA) as Proton-Conducting Membranes for Fuel Cells: Effect of Cross-Linking and Plasticizer Addition,” *ECS Trans*, vol. 53, pp. 29–34, 2013.

[28] R. Sood, S. Cavaliere, D. J. Jones, and J. Rozière, “Electrospun nanofibre composite polymer electrolyte fuel cell and electrolysis membranes,” *Nano Energy*, vol. 26, pp. 729–745, 2016.

[29] P.-Y. Hsu *et al.*, “Highly zeolite-loaded polyvinyl alcohol composite membranes for alkaline fuel-cell electrolytes,” *Polymers (Basel)*, vol. 10, no. 1, p. 102, 2018.

[30] Y. Zhao, H. Yu, D. Xing, W. Lu, Z. Shao, and B. Yi, “Preparation and characterization of PTFE based composite anion exchange membranes for alkaline fuel cells,” *J. Memb. Sci.*, vol. 421–422, pp. 311–317, 2012.

[31] J. R. Varcoe, R. C. T. Slade, E. Lam How Yee, S. D. Poynton, D. J. Driscoll, and D. C. Apperley, “Ethylene-Co-Tetrafluoroethylene)-Derived Radiation-Grafted Anion-Exchange Membrane with Properties Specifically Tailored for Application in Metal-Cation-Free Alkaline Polymer Electrolyte Fuel Cells,” *Chem. Mater*, vol. 19, pp. 2686–2693, 2007.

[32] A. M. Sajjan, H. G. Premakshi, and M. Y. Kariduraganavar, “Synthesis and characterization of GTMAC grafted chitosan membranes for the dehydration of low water content isopropanol by pervaporation,” *J. Ind. Eng. Chem.*, vol. 25, pp. 151–161, 2015.

[33] Y. Wan, B. Peppley, K. A. M. Creber, V. T. Bui, and E. Halliop, “Quaternized-chitosan membranes for possible applications in alkaline fuel cells,” *J. Power Sources*, vol. 185, no. 1, pp. 183–187, 2008.

[34] M. Mandal, G. Huang, and P. A. Kohl, “Anionic multiblock copolymer membrane based on vinyl addition polymerization of norbornenes: Applications in anion-exchange membrane fuel cells,” *J. Memb. Sci.*, vol. 570–571, pp. 394–402, 2019.

[35] G. Couture, A. Alaaeddine, F. Boschet, and B. Ameduri, “Polymeric materials as anion-exchange membranes for alkaline fuel cells,” *Prog. Polym. Sci.*, vol. 36, no. 11, pp. 1521–1557, 2011.

[36] B.-N. Lee, T. Y. Son, C. H. Park, T. H. Kim, and S. Y. Nam, “Preparation and characterization of various poly(ether ether ketone) containing imidazolium moiety for anion exchange membrane fuel cell application,” *J. Nanosci. Nanotechnol.*, vol. 18, no. 9, pp. 6447–6454, 2018.

[37] K. J. T. Noonan, K. M. Hugar, H. A. Kostalik IV, E. B. Lobkovsky, H. D. Abruña, and G. W. Coates, “Phosphonium-functionalized polyethylene: A new class of base-stable alkaline anion exchange membranes,” *J. Am. Chem. Soc*., vol. 134, no. 44, pp. 18161–18164, 2012.

[38] J. Cheng et al., “Guanidimidazole-quanternized and cross-linked alkaline polymer electrolyte membrane for fuel cell application,” *J. Memb. Sci.*, vol. 501, pp. 100–108, 2016.

[39] X. Tan et al., “Alkaline stable pyrrolidinium-type main-chain polymer: The synergetic effect between adjacent cations,” *J. Memb. Sci.*, vol. 618, no. 118689, p. 118689, 2021.

[40] M. A. Hossain et al., “Novel hydroxide conducting sulfonium-based anion exchange membrane for alkaline fuel cell applications,” *Int. J. Hydrogen Energy*, vol. 41, no. 24, pp. 10458–10465, 2016.

[41] H. Gopi and K. Bhat, “Anion Exchange Membrane from Polyvinyl Alcohol Functionalized with Quaternary Ammonium Groups via Alkyl Spacers,” *Ionics*, vol. 24, pp. 1097–1109, 2018.

[42] A. M. Samsudin, M. Roschger, S. Wolf, and V. Hacker, “Preparation and characterization of QPVA/PDDA electrospun nanofiber anion exchange membranes for alkaline fuel cells,” *Nanomaterials (Basel)*, vol. 12, no. 22, 2022.

[43] X. Du, H. Zhang, Y. Yuan, and Z. Wang, “Semi-interpenetrating network anion exchange membranes based on quaternized polyvinyl alcohol/poly(diallyldimethylammonium chloride),” *Green Energy Environ*., vol. 6, no. 5, pp. 743–750, 2021.

[44] D. Wang, Y. Wang, J. Wang, and L. Wang, “Synthesized Geminal-imidazolium-type ionic liquids applying for PVA-FP/[DimL][OH] anion exchange membranes for fuel cells,” *Polymer (Guildf.)*, vol. 170, pp. 31–42, 2019.

[45] J. Płotka-Wasylka, M. de la Guardia, V. Andruch, and M. Vilková, “Deep eutectic solvents vs ionic liquids: Similarities and differences,” *Microchem. J.*, vol. 159, no. 105539, p. 105539, 2020.

[46] Y. Chu, Y. Chen, N. Chen, F. Wang, and H. Zhu, “A new method for improving the ion conductivity of anion exchange membranes by using TiO2 nanoparticles coated with ionic liquid,” *RSC Adv.*, vol. 6, no. 99, pp. 96768–96777, 2016.

[47] M. B. Karimi, F. Mohammadi, and K. Hooshyari, “Potential use of deep eutectic solvents (DESs) to enhance anhydrous proton conductivity of Nafion 115® membrane for fuel cell applications,” *J. Memb. Sci.*, vol. 611, no. 118217, p. 118217, 2020.

[48] A. P. Abbott, G. Capper, D. L. Davies, K. J. McKenzie, and S. U. Obi, “Solubility of metal oxides in deep eutectic solvents based on choline chloride,” *J. Chem. Eng. Data*, vol. 51, no. 4, pp. 1280–1282, 2006.

[49] Y. Chen, D. Yu, W. Chen, L. Fu, and T. Mu, “Water absorption by deep eutectic solvents,” *Phys. Chem. Chem. Phys.*, vol. 21, no. 5, pp. 2601–2610, 2019.

[50] A. I. Dudu, L. C. Bencze, C. Paizs, and M. I. Toşa, “Deep eutectic solvents – a new additive in the encapsulation of lipase B from Candida antarctica: biocatalytic applications,” *React. Chem. Eng.*, vol. 7, no. 2, pp. 442–449, 2022.

[51] E. L. Smith, A. P. Abbott, and K. S. Ryder, “Deep eutectic solvents (DESs) and their applications,” *Chem. Rev.*, vol. 114, no. 21, pp. 11060–11082, 2014.

[52] Y. Dai, J. van Spronsen, G.-J. Witkamp, R. Verpoorte, and Y. H. Choi, “Natural deep eutectic solvents as new potential media for green technology,” *Anal. Chim. Acta*, vol. 766, pp. 61–68, 2013.

[53] M. A. Kareem, F. S. Mjalli, M. A. Hashim, and I. M. AlNashef, “Phosphonium-based ionic liquids analogues and their physical properties,” *J. Chem. Eng. Data*, vol. 55, no. 11, pp. 4632–4637, 2010.

[54] D. Carriazo, M. C. Serrano, M. C. Gutiérrez, M. L. Ferrer, and F. del Monte, “Deep-eutectic solvents playing multiple roles in the synthesis of polymers and related materials,” *Chem. Soc. Rev.*, vol. 41, no. 14, pp. 4996–5014, 2012.

[55] L. I. N. Tomé, V. Baião, W. da Silva, and C. M. A. Brett, “Deep eutectic solvents for the production and application of new materials,” *Appl. Mater. Today*, vol. 10, pp. 30–50, 2018.

[56] M. A. Kareem, F. S. Mjalli, M. A. Hashim, M. K. O. Hadj-Kali, F. S. G. Bagh, and I. M. Alnashef, “Phase equilibria of toluene/heptane with tetrabutylphosphonium bromide based deep eutectic solvents for the potential use in the separation of aromatics from naphtha,” *Fluid Phase Equilib.*, vol. 333, pp. 47–54, 2012.

[57] T. El Achkar, H. Greige-Gerges, and S. Fourmentin, “Basics and properties of deep eutectic solvents: a review,” *Environ. Chem. Lett.*, vol. 19, no. 4, pp. 3397–3408, 2021.

[58] R. Castro-Muñoz, F. Galiano, A. Figoli, and G. Boczkaj, “Deep eutectic solvents – A new platform in membrane fabrication and membrane-assisted technologies,” *J. Environ. Chem. Eng.*, vol. 10, no. 2, p. 106414, 2022.

[59] J. Serna-Vázquez, M. Z. Ahmad, G. Boczkaj, and R. Castro-Muñoz, “Latest insights on novel deep eutectic solvents (DES) for sustainable extraction of phenolic compounds from natural sources,” *Molecules*, vol. 26, no. 16, p. 5037, 2021.

[60] A. P. Abbott, S. Nandhra, S. Postlethwaite, E. L. Smith, and K. S. Ryder, “Electroless deposition of metallic silver from a choline chloride-based ionic liquid: a study using acoustic impedance spectroscopy, SEM and atomic force microscopy,” *Phys. Chem. Chem. Phys.*, vol. 9, no. 28, p. 3735, 2007.

[61] N. Peeters, K. Janssens, D. de Vos, K. Binnemans, and S. Riaño, “Choline chloride–ethylene glycol based deep-eutectic solvents as lixiviants for cobalt recovery from lithium-ion battery cathode materials: are these solvents really green in high-temperature processes?,” *Green Chem.*, vol. 24, no. 17, pp. 6685–6695, 2022.

[62] M. Jablonský, A. Škulcová, and J. Šima, “Use of deep eutectic solvents in polymer chemistry–A review,” *Molecules*, vol. 24, no. 21, p. 3978, 2019.

[63] S. Seyyed Shahabi, N. Azizi, and V. Vatanpour, “Tuning thin-film composite reverse osmosis membranes using deep eutectic solvents and ionic liquids toward enhanced water permeation,” *J. Memb. Sci.*, vol. 610, no. 118267, p. 118267, 2020.

[64] S. M. Rahman, S. B. Mohd Said, B. Subramanian, B. D. Long, M. A. Kareem, and N. Soin, “Synthesis and characterization of polymer electrolyte using deep eutectic solvents and electrospun poly(vinyl alcohol) membrane,” *Ind. Eng. Chem. Res.*, vol. 55, no. 30, pp. 8341–8348, 2016.

[65] F. Mano et al., “Production of poly(vinyl alcohol) (PVA) fibers with encapsulated natural deep eutectic solvent (NADES) using electrospinning,” *ACS Sustain. Chem. Eng.*, vol. 3, no. 10, pp. 2504–2509, 2015.

[66] C. Y. Wong, W. Y. Wong, R. Walvekar, K. S. Loh, M. Khalid, and K. L. Lim, “Effect of deep eutectic solvent in proton conduction and thermal behaviour of chitosan-based membrane,” *J. Mol. Liq.*, vol. 269, pp. 675–683, 2018.

[67] K. B. Rufato et al., “Electrospinning of poly(vinyl alcohol) and poly(vinyl alcohol)/tannin solutions: A critical viewpoint about crosslinking,” *Mater. Today Commun.*, vol. 35, no. 106271, p. 106271, 2023.

[68] S. H. Tan, A. L. Ahmad, M. G. M. Nawawi, and H. Hassan, “Performance of membranes crosslinked with glutaraldehyde in pervaporation separation,” *ASEAN J. Sci. Technol. Dev.*, vol. 19, no. 2, pp. 69–83, 2017.

[69] X. H. Yan, T. S. Zhao, G. Zhao, L. An, and X. L. Zhou, “A hydrophilic-hydrophobic dual-layer microporous layer enabling the improved water management of direct methanol fuel cells operating with neat methanol,” *J. Power Sources*, vol. 294, pp. 232–238, 2015.

[70] A. Mahto et al., “Sustainable water reclamation from different feed streams by forward osmosis process using deep eutectic solvents as reusable draw solution,” *Ind. Eng. Chem. Res.*, vol. 56, no. 49, pp. 14623–14632, 2017.

[71] S.-C. Jang, F.-S. Chuang, W.-C. Tsen, and T.-W. Kuo, “Quaternized chitosan/functionalized carbon nanotubes composite anion exchange membranes,” *J. Appl. Polym. Sci.*, vol. 136, no. 30, 2019.

[72] H. Çabuk, Y. Yılmaz, and E. Yıldız, “Vortex-assisted deep eutectic solvent-based liquid-liquid microextraction for the analysis of alkyl gallates in vegetable oils,” *Acta Chim. Slov.*, vol. 66, no. 2, pp. 385–394, 2019.

[73] F. S Matty, M. T. Sultan, and A. K. Amine, “Swelling behavior of cross-link PVA with glutaraldehyde,” *Ibn Al-Haitham Journal For Pure and Applied Sciences*, vol. 28, no. 2, pp. 136-146, 2015.

[74] A. A. I. Velez, E. Reyes, A. Diaz-Barrios, F. Santos, A. J. Fernández Romero, and J. P. Tafur, “Properties of the PVA-VAVTD KOH blend as a gel polymer electrolyte for zinc batteries,” *Gels*, vol. 7, no. 4, p. 256, 2021.

[75] N. Delgado-Mellado et al., “Thermal stability of choline chloride deep eutectic solvents by TGA/FTIR-ATR analysis,” *J. Mol. Liq.*, vol. 260, pp. 37–43, 2018.

[76] A. M. Samsudin and V. Hacker, “Preparation and characterization of PVA/PDDA/nano-Zirconia composite anion exchange membranes for fuel cells,” *Polymers (Basel)*, vol. 11, no. 9, p. 1399, 2019.

[77] J. R. Brusas and E. M. B. Dela Pena, “Hygroscopicity of 1:2 choline chloride:Ethylene glycol deep eutectic solvent: A hindrance to its electroplating industry adoption,” *J. Electrochem. Sci. Technol.*, vol. 12, no. 4, pp. 387–397, 2021.